




Review: recent progress in low-temperature proton-conducting ceramics

Yuqing Meng¹, Jun Gao¹, Zeyu Zhao¹, Jake Amoroso², Jianhua Tong¹, and Kyle S. Brinkman^{1,3,*} 

¹Department of Materials Science and Engineering, Clemson University, Clemson, SC 29634, USA

²Savannah River National Laboratory, Aiken, SC 29808, USA

³Center for Nuclear Environmental Engineering Sciences and Radioactive Waste Management (NEESRWM), Clemson University, Clemson, SC 29634, USA

Received: 27 January 2019

Accepted: 20 March 2019

Published online:
9 April 2019

© The Author(s) 2019

ABSTRACTS

Proton-conducting ceramics (PCCs) are of considerable interest for use in energy conversion and storage applications, electrochemical sensors, and separation membranes. PCCs that combine performance, efficiency, stability, and an ability to operate at low temperatures are particularly attractive. This review summarizes the recent progress made in the development of low-temperature proton-conducting ceramics (LT-PCCs), which are defined as operating in the temperature range of 25–400 °C. The structure of these ceramic materials, the characteristics of proton transport mechanisms, and the potential applications for LT-PCCs will be summarized with an emphasis on protonic conduction occurring at interfaces. Three temperature zones are defined in the LT-PCC operating regime based on the predominant proton transfer mechanism occurring in each zone. The variation in material properties, such as crystal structure, conductivity, microstructure, fabrication methods required to achieve the requisite grain size distribution, along with typical strategies pursued to enhance the proton conduction, is addressed. Finally, a perspective regarding applications of these materials to low-temperature solid oxide fuel cells, hydrogen separation membranes, and emerging areas in the nuclear industry including off-gas capture and isotopic separations is presented.

Introduction

Protonic species (H^+) require a lower activation energy to transport through solid-state crystal structures and associated interfaces due to the small ionic radius and the absence of an electron cloud as

compared to other conducting ionic species such as oxygen ions (O^{2-}) [1]. Due to the combination of performance, efficiency, and stability in the lower temperature range, proton-conducting ceramics (PCCs) have attracted significant interest for applications in energy conversion [2–8], energy storage [9],

Address correspondence to E-mail: ksbrink@clemson.edu

electrochemical sensors [10], and advanced gas separations [11–15]. In addition, there has been recent interest in PCCs as enabling technologies in the nuclear industry, including their use as PCCs for tritium sequestration, electrolysis, and separations [16].

Conventional materials used for solid oxide fuel cells (SOFCs) electrolytes are typically oxygen-ion-conducting ceramics operated in a high temperature range (HT, 700–1000 °C). Degradation occurring at these temperatures and difficulties in high-temperature sealing of ceramic, glass, and metal components are the main causes for the limited solid oxide fuel cell (SOFC) commercialization at the present time. The high operating temperatures require the use of expensive interconnect materials, large energy input, and long start-up times [17]. This has driven the need for materials that produce a reasonable power output at intermediate temperatures (IT, 400–700 °C) [1]. The lower activation energy of PCC materials has made them attractive candidates for electrolyte materials operating in the IT range (400–700 °C). Numerous research works and several review papers on PCCs have recently focused on this IT range [1, 18, 19]. Zhang et al. [20] reviewed recent advances in SOFC materials and key components operating around 500 °C, with a focus on the materials, structures, and technique development for IT-SOFCs. A recent book on proton-conducting ceramics was published in 2016 [21], which covered the fundamentals of proton hydration, transport properties, and some typical applications in the temperature range higher than 350 °C. Kochetova et al. [22] thoroughly reviewed the PCC materials and applications at temperatures higher than 400 °C. However, the further reduction in operating temperature (e.g., < 400 °C) can further reduce system costs due to the wider range of material candidates for interconnects as well as the reduced balance of plant (BOP) costs. In addition, the long-term durability can also be improved by operating at decreased temperatures. In principle, the theoretical fuel cell efficiency can also be increased by reducing operating temperature [23].

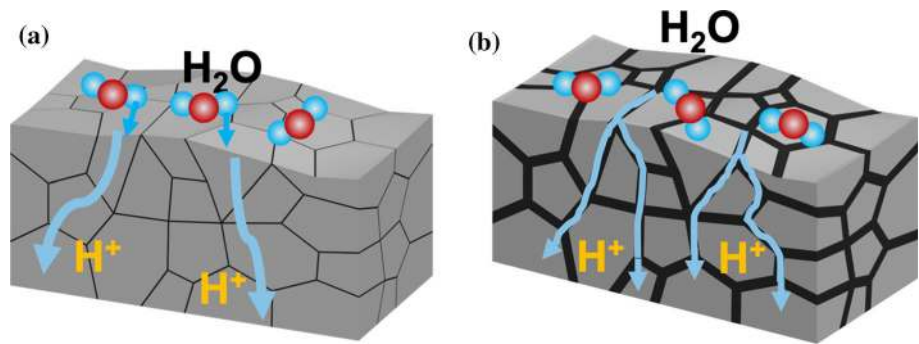
In the past decade, some promising proton-conducting properties have been reported at temperatures lower than 400 °C, with some of these studies even reporting room-temperature (RT) proton conduction. A common theme in the reports of low-temperature proton conduction was the presence of nanometer-size grains resulting in enhanced grain

boundary interfacial area. Furthermore, the electrical nature of these grain boundaries in nanostructured ionic conductors at low temperature has attracted considerable attention [24–26]. Park et al. [27] prepared nanostructured yttrium-doped barium zirconate ($\text{BaZr}_{0.9}\text{Y}_{0.1}\text{O}_3$) and investigated its grain and grain boundary protonic conductivity from RT to 400 °C. Unexpectedly, high proton conduction was observed at low temperatures (< 100 °C) in the nanostructure. At the same time, interfacial proton conductivity in LT range has also been observed in simple oxide systems such as yttria-stabilized zirconia (YSZ) [28–31], ceria [25, 32–36], titania [37] which do not exhibit bulk proton conduction in the IT range. Miyoshi et al. [28] reported that the interfacial protonic conduction in nanostructured YSZ became noticeably high when the grain size was smaller than 100 nm and increased dramatically with decreasing grain size. The origin of the proton conductivity in these systems has been attributed to absorbed water at the grain boundary interfaces. The mechanisms of interfacial conduction have been used to describe LT conduction behavior and are schematically shown in Fig. 1. It is emphasized that the proton transport property is particular to its nanostructure that consists of nanograins connected with the interfacial hydrated layer, which serves as the pathway for interfacial protonic conduction rather than transport through bulk which occurs in the IT to HT regime.

In addition, several new classes of ceramic materials have been discovered to behave as proton conductors in the LT range: (1) Gui et al. [38] utilized the layered structure of phosphates to construct channels facilitating proton conduction below 300 °C, (2) new SiO_2 -based composites have been found to exhibit proton conduction at room temperature [39], (3) Liu et al. [40] converted a lithium conductor to a proton conductor by ion exchange at low temperatures, and (4) Zhou et al. [41] devised a new doping strategy (electron doping) to develop high-performance SmNiO_3 (SNO) perovskite proton conductors for LT solid oxide fuel cells.

Due to the growing number of researchers reporting details of interfacial proton conduction in LT-PCCs, a systematic review would be useful given the large number of published works and recent scientific developments. This work fills the gap by providing review on proton-conducting ceramics in low temperature (LT, 25–400 °C). Based on a review of the literature, three temperature zones are defined in

Figure 1 Schematic illustrations of hydrogen permeation **a** through a bulk material and **b** assisted by a hydrated, intergranular layer (interfacial conduction) that acts as a rapid transport pathway.



the LT-PCC operating regime based on the predominant proton transfer mechanism occurring in each zone. The variation in material properties such as crystal structure, conductivity, microstructure, fabrication methods required to achieve the requisite grain size distribution, along with typical strategies pursued to enhance the proton conduction is addressed. Finally, a perspective regarding applications of these materials to low-temperature (LT) solid oxide fuel cells, hydrogen separation membranes, and emerging areas in the nuclear industry including off-gas capture and isotopic separations is presented.

Proton conduction at low temperature

There are four possible proton transport pathways in PCCs: (1) transport in the bulk, (2) transport along the grain boundaries (GBs), (3) transport on the open pores surfaces in the absorbed water layer, and (4) transport in a proton-enriched layer directly below the pore/oxide interface (see Fig. 2) [32]. Due to limited water adsorption on the grain boundary when the temperature is higher than 500 °C, proton conduction occurs mainly through bulk diffusion which has a smaller resistance than grain boundary diffusion. When the temperature is lower than 100 °C, the residual open porosity is the key factor for the proton conductivity due to the enhanced physisorption reaction of water which occurs in this temperature range.

The amount of water adsorbed on an oxide surface is described by Langmuir and BET theory which depends on the thermodynamics of the water adsorption reaction [42, 43]. Norby et al. [44] investigated the structure of an adsorbed water layer on surfaces of yttria-stabilized zirconia (YSZ) as a function of temperature and humidity. At 30% relative

humidity (RH), the water layer consisted of three monolayers; two chemisorbed water layers and one physisorbed water that in combination displayed an “ice-like” structure [45]. The chemisorbed water layer consisted of molecular adsorbed water hydroxyls which were stable up to temperatures near 600 °C and a hydrogen-bonded layer which was stable to temperature near 200 °C. From 30 to 60% RH, there occurred a transition between “ice-like” structure and “water-like” structures for the second chemisorbed layer. Above 60% RH, the water molecules were similar to free liquid water. The proton conductivity in LTs depends on the nanostructure (e.g., grain size, porosity), humidity, and temperature (Table 1, 2).

Hopping mechanism

The proton conductivity behaviors in wet environments as a function of temperature for several model ceramic materials consisting of simple oxides, fluoride-type oxides, and perovskite-type oxides are shown in Fig. 3. For comparison, the typical dependence of the electrical conductivity on temperature in dry air for a micrometric polycrystalline zirconia is also included in this figure as a solid line. Three distinct regimes of conductivity or zones can be evidenced which correspond to the predominant proton conduction mechanism operating in these temperature regimes. These three different regimes physically correspond to differences in chemically and physically adsorbed water molecules bound to the surface of the oxide grains: Zone 1 ($T < 50$ °C) occurs where physical adsorption of water dominates; zone 2 (50 °C $< T < 150$ °C) occurs where hydrogen bond network structure competes with physically adsorbed water; and zone 3 (150 °C $< T < 400$ °C) occurs where chemical adsorption prevails [29]. In zone 1 and zone 2, and apparent negative activation energy

Figure 2 **a** Schematic 2D representation of the microstructure of the porous nanocrystalline films. Four proton transport pathways are considered: 1 transport in the bulk, 2 along the GBs, 3 on the open pores surfaces in the adsorbed water layer, and 4 in a proton-enriched layer right below the pore/oxide interface. **b** Detail of pathway 3. **c** Detail of pathway 4. Reprinted with permission from Gregori et al. [32].

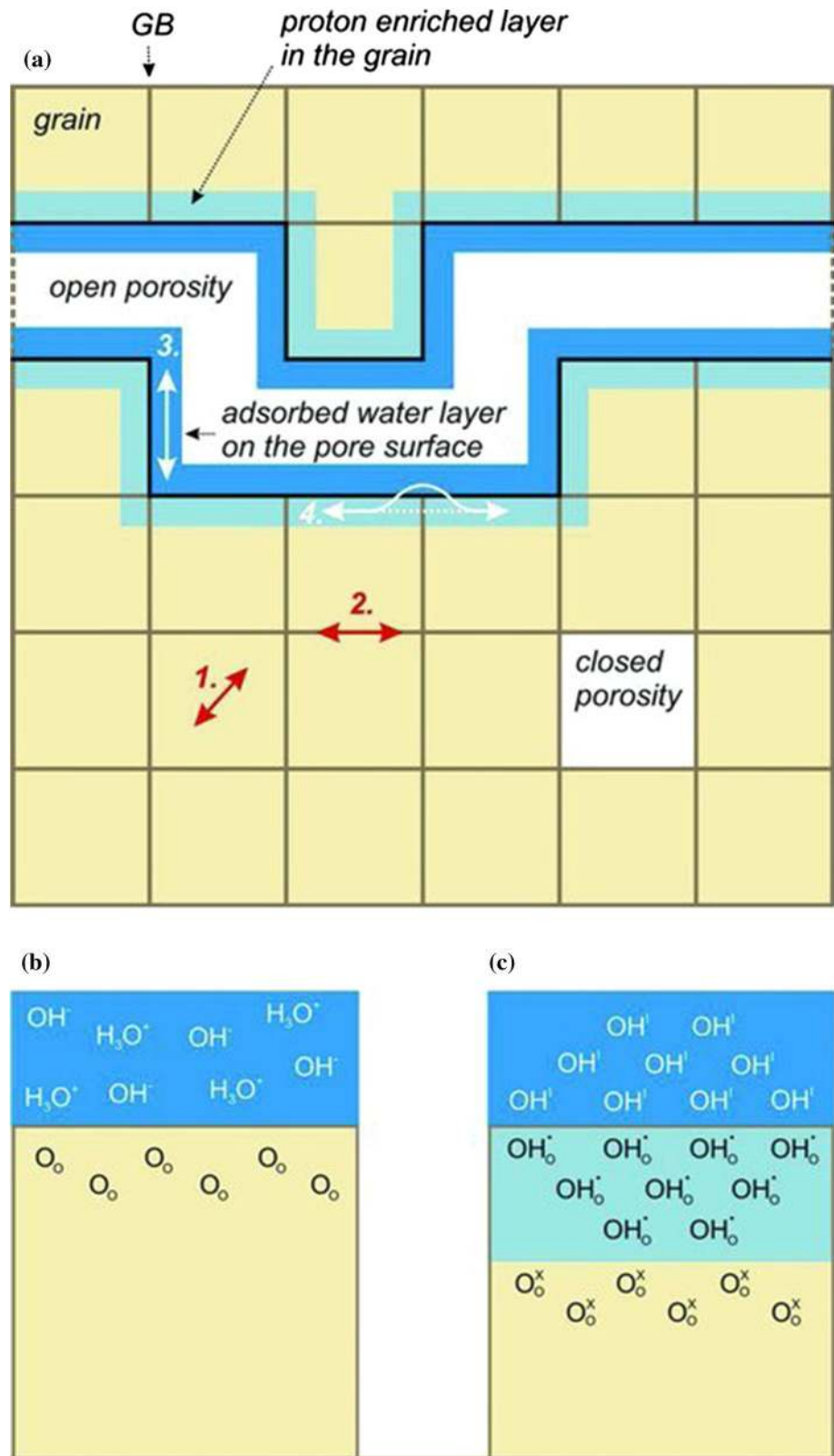


Table 1 Conductivity of doped perovskite-type proton conductors reported in the literature

Materials	Temp (°C)	Conductivity ^a (S/cm)	Measurement conditions	Activation Energy (eV)	References
BaZr _{0.25} In _{0.75} O _{3-δ}	300	Total: 9.2 × 10 ⁻⁵	Hydrated	Bulk: 0.4 Total: 0.63	[92]
BaZr _{0.9} Y _{0.1} O ₃	300	Gb: 8.7 × 10 ⁻⁴ Bulk: 1.4 × 10 ⁻³	Wet (10%)-Ar-O ₂	GB:0.7–0.8 Bulk: 0.63	[99]
BaZr _{0.9} Y _{0.1} O ₃	300	Gb: 3 × 10 ⁻⁴	Wet (2.3%)-air	GB:0.76 Bulk: 0.36	[100]
BaZr _{0.85} Y _{0.15} O ₃	350	Total:1.8 × 10 ⁻³	Wet (2.3%)-N ₂	0.43	[138]
Nano-BaZr _{0.8} Y _{0.2} O ₃	300	GB: 1.7 × 10 ⁻⁵	Wet (2.5%)-Ar	0.79	[101]
Ba _{0.97} Zr _{0.77} Y _{0.19} Zn _{0.04} O ₃	300	Total: 4.8 × 10 ⁻⁵	Wet-5%-Ar	N/A	[102]
BaCe _{0.9} Gd _{0.1} O ₃	300	Bulk: 3.1 × 10 ⁻⁴ GB: 1.1 × 10 ⁻⁶	Wet-Ar	Bulk: 0.53 GB: 0.75	[103]
BaCe _{0.8} Zr _{0.1} Gd _{0.1} O ₃	300	Bulk: 1.7 × 10 ⁻⁴ GB: 8.7 × 10 ⁻⁷	Wet-Ar	Bulk: 0.57 GB: 0.77	[103]
BaCe _{0.45} Zr _{0.45} Sc _{0.1} O ₃	325	Total: 2.5 × 10 ⁻⁶	Wet (5%)-H ₂ -Ar	0.67	[104]
SrCe _{0.95} Yb _{0.05} O ₃	300	Total: 2.7 × 10 ⁻⁵	Wet-Ar	Bulk: 0.6 GB: 0.81	[105]
Sr ₃ CaZr _{0.5} Ta _{1.5} O _{8.75}	300	Total: 5.5 × 10 ⁻⁵	Wet 4% H ₂ -Ar	Bulk: 0.66 GB: 0.85	[91]
BaCe _{0.65} Zr _{0.20} Y _{0.15} O _{3-δ}	300	Total: 4.4 × 10 ⁻⁴	Wet 5% H ₂ -Ar	Bulk: 0.6 GB: 0.92	[96]
Ba _{0.5} Sr _{0.5} Ce _{0.6} Zr _{0.2} Gd _{0.1} Y _{0.1} O _{3-δ}	300	Total: 9.5 × 10 ⁻⁴	Wet air	0.73	[90]

^aBulk conductivity refers to conduction through the grain interior portions of the sample only, where total refers to conduction through both the grain interiors and the grain boundaries

Table 2 Example of proton-conducting oxides with nanometric grain size

Materials	Sintering method	Grain size (nm)	Density (%)	Pressure (MPa)	Temperature (°C)	References
6 mol % Sm-doped ceria	HMTA/UV laser irradiation	2–3	N/A		50	[33]
YSZ	RT high-pressure compaction	< 100	86	4000	RT	[28]
Ce _{0.9} Gd _{0.1} O _{2-δ}	SPS	~ 120 nm	> 97	50	1000	[35]
YSZ	SPS	50	> 97	14–141	800–1000	[129]
TiO ₂	HP-FAST	24–56	92–95	800 MPa	550	[111]
TiO ₂	Hot pressing	30	90	450	490	[131]
TiO ₂	Two-stage sintering	100	N/A	0.1	750	[130]
BaTiO ₃	SPS	30	96	100	800	[134]
BaTiO ₃	High-pressure-assisted sintering	30	96.2	200	1000	[135]

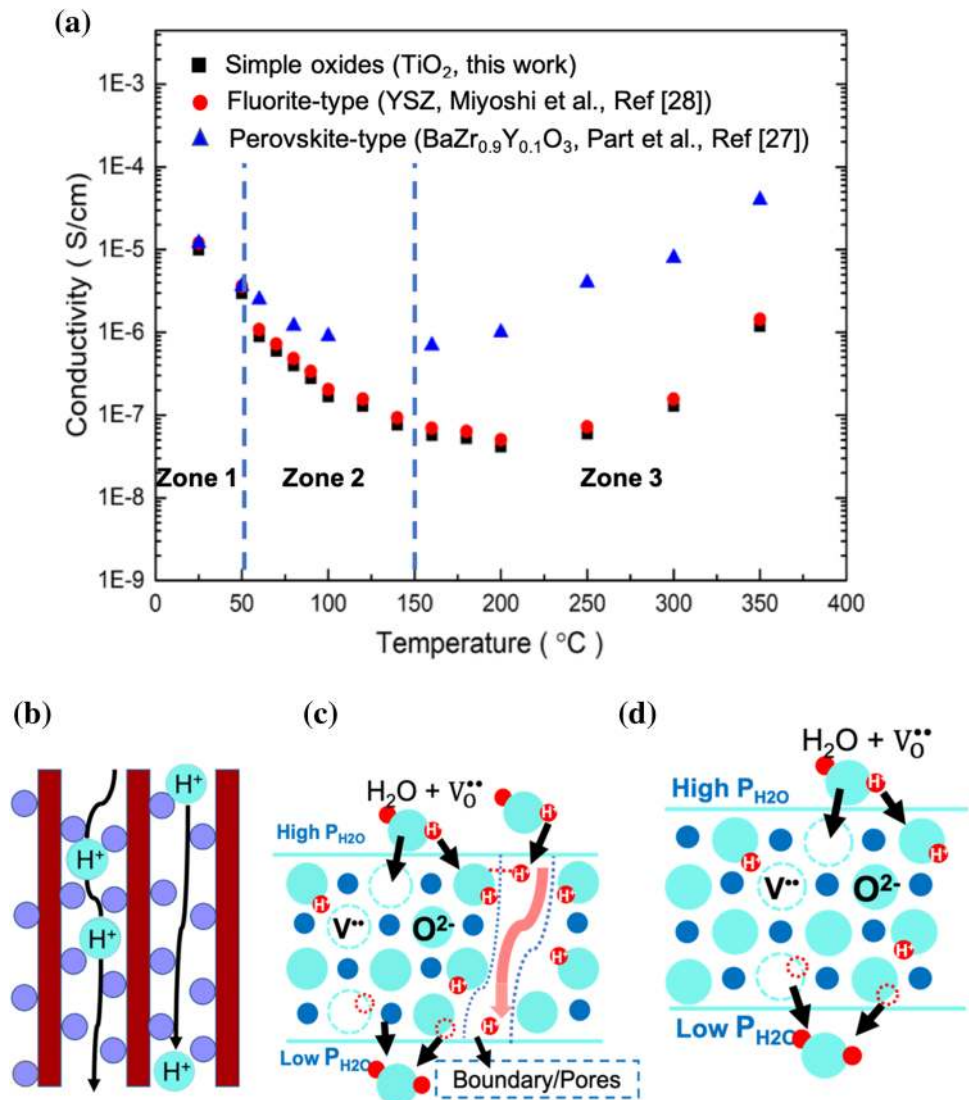
The detailed microstructures are shown in Fig. 11

is observed because the strong dependence of water adsorption on temperature. The transition of the conduction mechanism around 50 °C should be related to the condensation of water at lower temperature.

In zone 3, the conduction of protons can be generally described by the hopping (Grotthuss) mechanism, in which the protons strongly interact with the electron density of nearby electronegative oxygen ions. Proton transport is a thermally activated hopping process requiring the breaking and reforming of the O–H bond. Proton conduction by a hopping mechanism shows an important isotope effect which stems from a large difference in the mass of H⁺ and

D⁺ [46–48]. Nowick and Vaysleyb [49] described the theories concerning the isotope effect and resulting impact on proton conduction. The mass difference between hydrogen and deuterium affects their vibrational frequencies in the infrared regime of the compounds [50]. The classical model predicts that the rate of a proton hopping in an oxide is proportional to the attempt frequency or O–H/O–D vibration frequency. Therefore, the mobility of a proton should be larger than that of a deuteron by factor in the range 1.374–1.414, while the activation energies of the two species should be identical. Miyoshi et al. reported the extent of isotope effect ($\sigma(\text{H}_2\text{O})/\sigma(\text{D}_2\text{O})$) is around 2 to approximate the theoretical value of

Figure 3 **a** Overview of proton transport in nanocrystalline oxide materials: conductivity data for TiO_2 , $\text{BaZr}_{0.9}\text{Y}_{0.1}\text{O}_3$ [27], and YSZ [28] selected as representative of simple oxides, fluorite-type oxides, and perovskite-type oxides, respectively. **b** Schematic illustrations showing proton transport via interfacial conduction (zone 1), **c** proposed proton transport paths in zone 2, and **d** proposed transport of the proton in a perovskite-type material in zone 3.



1.4, indicating hopping-type mechanism of proton conduction.

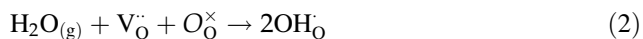
Schematically shown in Fig. 3c is the proposed hopping mechanism of protons, which requires two steps: (1) fast rotation of the protons located on the oxygen ion and (2) proton transfer via hopping toward a neighboring oxygen ion. Proton rotation is associated with a very low activation barrier below 0.1 eV [51], while proton transfer is slower and more difficult. According to the Grotthuss mechanism, the activation energy for proton migration is usually above 0.5 eV, indicating that proton jumps between the two adjacent oxygen ions which is the rate-determining step. In zone 3, perovskite-type oxides have the highest conductivity due to the fact that they can simultaneously possess protonic (H^+) and

oxygen ionic (O^{2-}) conductivity. Moreover, their total conductivities strongly depend on the factors such as temperature, microstructure, oxygen and water vapor partial pressure, and bulk/grain boundary transport. In this temperature range, grain boundary conduction remains a highly resistive mechanism even in nanostructured materials as demonstrated by Park et al. [27] for nanostructured Y-doped BaZrO_3 .

Protons can be incorporated into the bulk of the perovskite structure as hydroxyl defects (OH_O) in the presence of hydrogen and/or water vapor-containing gases. If surrounding the proton conductor with a dry hydrogen atmosphere, the formation of hydroxyl defects occurs through the following reaction:



whereas the most important reaction leading to the formation of hydroxide defects is considered to be the dissociative adsorption of water in humidified atmosphere [52–58]. Proton defects are formed by the dissociative absorption of water at the surface, which requires the presence of oxygen vacancies. Water molecules dissociate into hydroxyl groups (OH^-) and protons (H^+), with hydroxyl groups incorporated into oxygen vacancies, while the protons form a covalent bond with a lattice oxygen. The reaction can be written in Kröger–Vink notation:



The energy of water incorporation into perovskite oxides has been found to be exothermic, and incorporation of water in doped systems is more exothermic than in undoped systems [59]. This is in good agreement with the observation that proton uptake in perovskite material increases with decreasing temperature in the low temperature range [60].

Protonic conductivity abruptly increased at lower ($50^\circ\text{C} < T < 150^\circ\text{C}$, zone 2). The hopping mechanism was predominant in this zone. The temperature dependence of the conductivity in this temperature range shows a strong negative activation energy, which can be ascribed to the strong dependence of the amount of absorbed water on temperature [44].

Interfacial conduction mechanism

Enormous efforts have been devoted to developing a protonic conductor with high proton conductivity. In recent years, nanostructured materials have been employed as a way to enhance the low-temperature proton conductivity [29, 61]. Guo et al. [62] first investigated the water effect on conduction by fabricating a nanocrystalline YSZ film. Anselmi-Tamburini et al. [63] measured the proton conductivity of nanostructured YSZ (15 nm) which was fabricated using spark plasma sintering at low temperature. A recent study suggested that the protonic transport mechanism in YSZ changes from Grotthuss-type diffusion at high temperatures and low water content to vehicle-type diffusion (H_3O^+) at lower temperature and higher water content [28]. In the low temperature range (zone 1), the differences between the conductivity in simple oxides and the complex

materials become negligible. The nanocrystalline materials show a strong hydration (water uptake) behavior in zone 1, and absorbed water layers on the surface and grain boundary are considered to be the possible path for such a low-temperature proton transport [27]. The transition of the conduction mechanism around 50°C should be related to the capillary condensation of water at lower temperature.

Surface termination and structural features are also important in addition to increased overall interfacial area. Taking YSZ as an example, we emphasize that in zone 1, zirconium and oxygen atoms act as Lewis acid and base sites, respectively [64]. The water adsorption calculations show that the (111) surface of YSZ is favorable for the dissociative adsorption of water [65]. Adsorbed water dissociated on the bare surface of the ZrO_2 -based oxides to form hydroxyl groups on the surface, and the pK_a of those hydroxyl groups was found to range between 10 and 13, reported by Tret'yakov et al. [66]. In addition, the enthalpy of the hydroxylation reaction was reported to be rather high, suggesting the instability of the bare surface [67]. These chemical surface features of hydroxyl and H_2O molecules on the ZrO_2 -based oxide surface would be expected to facilitate the proton conduction. In contrast to micrometer grains, nanograins tend to involve disordered surface and dangling bonds, which leads to an increased instability of the bare surface and finally gives rise to room-temperature proton conduction of nanograined materials which occurs due to enhanced water absorption and dissociation.

Microstructural effects

Malavasi et al. pointed out that nanoscale materials exhibit significant size effects due to short diffusion lengths and a high density of interfaces resulting in effective properties of the material dominated by the grain boundary interfaces [59, 68]. It is generally recognized that proton incorporation into proton conductors (for instance, perovskite oxides) occurs by a two-step process [57, 69–71], and both bulk and grain boundary contribute to the total conductivity. Therefore, the materials microstructure has a significant effect on the electrical properties of these materials. Ionic transport in PCC materials is controlled by the grain boundary phase, which generally acts as a “blocking” layer against ionic transport in polycrystalline materials sintered with micron-size grains.

However, recent research suggests that the size and structure of the grain boundary can be tailored to affect the behavior of proton transport at interfaces, especially in the low-temperature (LT) regime.

Several authors have called attention to nanoscale materials as a means to design PCCs dominated by grain boundary interfaces. The size effect of nanodomains in these materials can be effectively controlled to fabricate materials with a high density of interfaces but short diffusion lengths, resulting in favorable conduction properties [59, 68]. Indeed, nanostructured materials have been employed as a way to enhance low-temperature proton conductivity [29, 61]. Anselmi-Tamburini et al. [63] measured the proton conductivity of nanostructured YSZ (15 nm) fabricated using spark plasma sintering (SPS) at low temperature. Guo et al. [62] first investigated the water effect on conduction by making a nanocrystalline YSZ film. More recently, Miyoshi et al. have reported notable interfacial protonic conduction in nanostructured YSZ with grain sizes less than 100 nm, which increases dramatically with decreasing grain size. For example, the conductivity increased by three orders of magnitude when reducing the grain size from 100 to 13 nm at RT. This group suggested a vehicle-type proton transport mechanism in LTs which is proved by disappearance of isotope effect [28].

Haile et al. [72] investigated the influence of grain boundary conductivity and microstructure on the electrical properties of $\text{BaCe}_{0.85}\text{Gd}_{0.15}\text{O}_{3-\delta}$, and the grain size was controlled by sintering at various temperatures (Fig. 4). In this study, ‘brick layer model’ was used to calculate the grain interior and grain boundary conductivities [73, 74]. Their results indicated that the grain boundaries 22-03-2019 10:10:00 in barium cerate are significantly more resistive than the bulk, and the specific grain boundary conductivity is independent of grain size. Similar result was found by Braun et al. [75]: The activation energy for proton transport in the bulk and grain boundary of $\text{BaZr}_{0.9}\text{Y}_{0.1}\text{O}_{3-\delta}$ was 0.46 eV and 1.21 eV, respectively. The origin of the large resistance in grain boundary layer is manifested in the space charge depletion layers near the positively charged grain boundary core [76], where charge transport across the grain boundaries is blocked by depletion of the major charge carriers (H^+ , h , V_{O}) in the space charge zones.

The space charge effect, which is primarily governed by the electrochemical potential of the defect through the grain boundary and grain interior [77], is an inherent material property and shows a strong positive correlation with temperature. Thus, we consider the space charge effect can only have significant effect on the proton conductivity of grain boundaries in zone 3. A space charge effect on grain boundary conduction behavior based on the brick layer model has been suggested and experimentally examined [78]. As a result of this effect, the ionic charge carrier depletes and accumulates in the vicinity (space charge zone) of the grain boundary core. Such a depletion/accumulation of charge carriers is attributed to the existence of excess charge of the grain boundary core, which is inevitably formed due to thermodynamic difference between the grain boundary core and bulk [79, 80].

Kim et al. [30] investigated the resistivity of nano-YSZ with different grain sizes (13–100 nm) under water-saturated air. At temperature range higher than 200 °C (O region), the proton transport was found to be negligible in comparison with oxygen-ion transport, whereas the nano-YSZ becomes a proton conductor below ~ 120 °C (H region) in water-saturated air (see Fig. 4). More importantly, the total resistance decreases dramatically with decreasing grain size, indicating the leading role of the interface for the determination of proton conduction in nano-YSZ at low temperatures. The grain boundaries in YSZ are recognized to conduct ions selectively, which

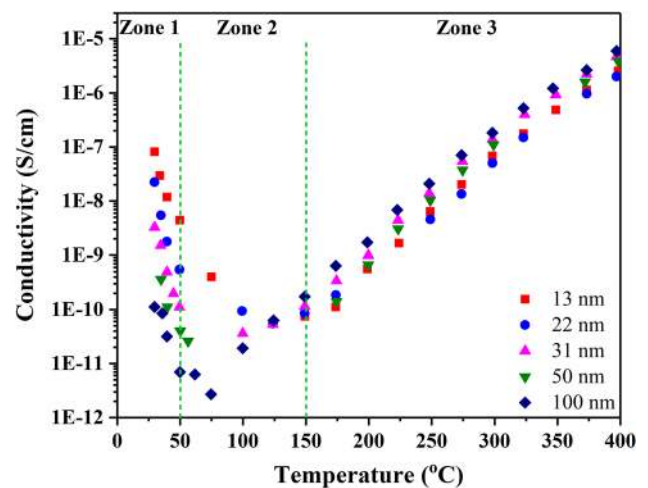


Figure 4 Total conductivity of nano-YSZ with different grain sizes measured under water-saturated air as a function of temperature. Reprinted with permission from Kim et al. [30].

may provide conductive paths for proton transport while hindering oxygen-ion transport [81–83]. The same selective nature of grain boundaries was also found in nanocrystalline mixed conducting ceria [84, 85].

LT-PCC materials

Perovskite type

BaCeO₃ was the first perovskite-type oxide found to exhibit proton conduction. Iwahara et al. [69] demonstrated this cubic structured material to be a potential electrolyte material in SOFCs. After more than 20 years of research, the perovskite-type cerates and zirconates have become well-established proton-conducting systems [71, 86–88]. The ideally packed perovskite structure is considered simple cubic structure. It has a space group PM-3 m, and the sites corresponding to the A cation are located at the vertices of the unit cell, B site cation in the center, and oxygen ions at the faces. The A site is occupied by alkaline earth elements, such as Sr, Ba, Ca, while the B site is occupied by tetravalent elements, e.g., Ce and Zr. Since oxygen vacancy plays an important role in the formation of mobile protons, it is paramount to dope the B site with suitable trivalent elements, such as Y, Yb, Sm, Nd, In, Gd.

Figure 5 shows a schematic illustration of a possible proton conduction mechanism in perovskite-type materials which takes place in zone 3. Firstly, protons migrate from oxygen ion I to oxygen ion II (form position 1 to position 2). Then, fast rotational motion of the protons occurs on the oxygen ion II (from 2 to 3). Shown in Fig. 6 are the total conductivities in perovskite-type proton conductors under wet atmosphere as a function of temperature. In zone 3, the proton conduction mechanism occurs by proton hopping between adjacent oxygen ions which was proved by isotope-effect measurements. It is reported that structural distortion and chemical perturbations induced by cation doping can influence the proton conduction [89]. In general, deviation from the ideal cubic perovskite structure mainly leads to a large activation energy.

Pure, undoped BaCeO₃, SrCeO₃, and SrZrO₃ have limited oxygen vacancy concentrations which leads to low proton incorporation. BaCeO₃-based materials exhibit good proton conductivity under a humidified

hydrogen-containing atmosphere, but rather poor chemical stability in CO₂ atmosphere. Replacement of Zr⁴⁺/Ce⁴⁺ with trivalent cations (e.g., Y³⁺) was demonstrated to be a feasible method to increase oxygen vacancy concentration. Singh et al. [90] investigated the chemical stability of Ba_{0.5}Sr_{0.5}Ce_{1-x-y-z}Zr_xGd_yY_zO_{3-δ} (0 < x < 0.5; y = 0, 0.1, 0.15; z = 0.1, 0.2) system. Among these materials, Ba_{0.5}Sr_{0.5}Ce_{0.6}Zr_{0.2}Gd_{0.1}Y_{0.1}O_{3-δ} (BSCZGY3) had the highest conductivity 9.5 × 10⁻⁴ S/cm at 300 °C under wet air (3% H₂O) atmosphere with an activation energy of 0.73 eV. Shuai Wang et al. [18] investigated the electrical properties of BaCe_{0.8}Y_{0.2-x}Nd_xO_{3-δ} (x = 0, 0.05, 0.10, 0.15), which exhibits the highest conductivity when x = 0.05(BCYN5). The SEM observation indicates that the densification and grain size of the sintered pellets were significantly enhanced with an increase in Nd doping concentration. Electrochemical impedance spectra (EIS) demonstrated that both bulk and grain boundary resistances decrease due to the synergistic effect of Nd and Y doping at 350 °C.

Conventional perovskite materials only exhibit appreciable levels of proton conduction at high temperature of 500 °C or above. Recently, newer generation of perovskite compositions has demonstrated impressive conductivity in the LT range. Irvine et al.

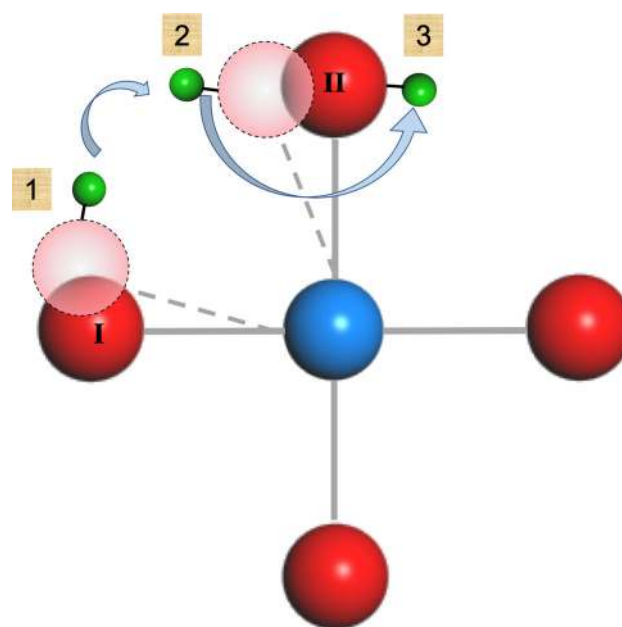
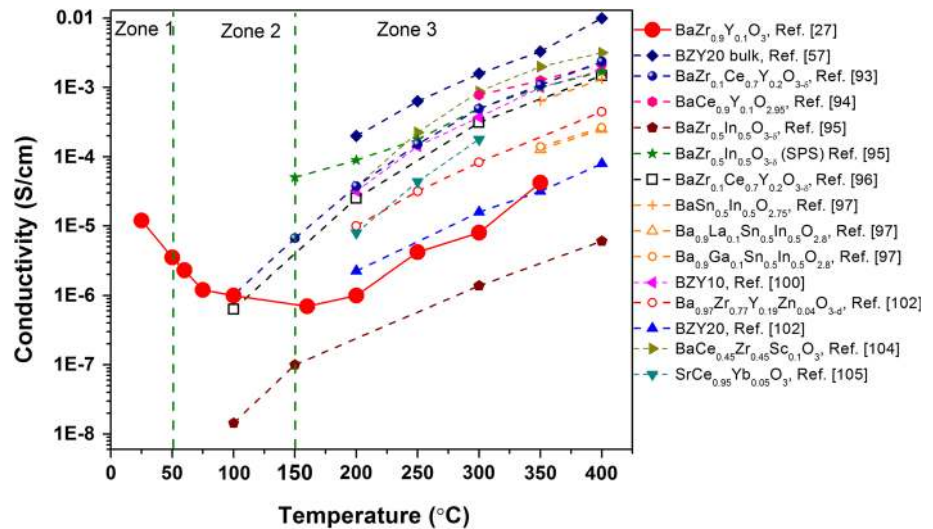


Figure 5 Schematic illustration of possible proton transfer mechanism in perovskite-type materials. Red atoms: oxygen, blue: transition metal, green: protons.

Figure 6 Total conductivities in perovskite-type proton conductors under wet atmosphere as a function of temperature. $\text{BaZr}_{1-x}\text{In}_x\text{O}_{3-\delta}$, $x = 0.75$ [92], $\text{BaZr}_{0.1}\text{Ce}_{0.7}\text{Y}_{0.2}\text{O}_{3-\delta}$ [93], $\text{BaCe}_{0.9}\text{Y}_{0.1}\text{O}_{2.95}$ [94], $\text{BaZr}_{0.5}\text{In}_{0.5}\text{O}_{3-\delta}$ [95], $\text{Sr}_3\text{CaZr}_{0.5}\text{Ta}_{1.5}\text{O}_{8.75}$ [91], $\text{BaCe}_{0.65}\text{Zr}_{0.20}\text{Y}_{0.15}\text{O}_{3-\delta}$ [96], $\text{BaSn}_{0.5}\text{In}_{0.5}\text{O}_{2.75}$, $\text{Ba}_{0.9}\text{La}_{0.1}\text{Sn}_{0.5}\text{In}_{0.5}\text{O}_{2.8}$, $\text{Ba}_{0.9}\text{Gd}_{0.1}\text{Sn}_{0.5}\text{In}_{0.5}\text{O}_{2.8}$ [97].



[91] reported a triple-perovskite $\text{Sr}_3\text{CaZr}_{0.5}\text{Ta}_{1.5}\text{O}_{8.75}$ as a proton-conducting oxide. The bulk and grain boundary conductivities of $\text{Sr}_3\text{CaZr}_{0.5}\text{Ta}_{1.5}\text{O}_{8.75}$ were found to be 4.64×10^{-4} and 7.04×10^{-5} S/cm, respectively, at 300 °C with activation energy of $E_{\text{bulk}} = 0.66$ eV and $E_{\text{gb}} = 0.85$ eV.

B-site substitution has been commonly used to modify physicochemical properties of proton-conducting perovskite-type oxides. A-site doping of +3 cations has been studied to a lesser degree because it is expected to introduce a positive charge, leading to a decreased oxygen vacancy concentration. Swierczek et al. [97] investigated the proton transport property of $\text{BaSn}_{0.5}\text{In}_{0.5}\text{O}_{2.75}$, $\text{Ba}_{0.9}\text{La}_{0.1}\text{Sn}_{0.5}\text{In}_{0.5}\text{O}_{2.75}$ and $\text{Ba}_{0.9}\text{Gd}_{0.1}\text{Sn}_{0.5}\text{In}_{0.5}\text{O}_{2.75}$. La- and Gd-containing compounds show smaller unit cell parameters compared to $\text{BaSn}_{0.5}\text{In}_{0.5}\text{O}_{2.75}$ due to the smaller ionic diameter as compared to Ba^{2+} -substituted compounds. $\text{BaSn}_{0.5}\text{In}_{0.5}\text{O}_{2.75}$ was expected to have highest proton conductivity since the proton conductivity is typically higher for the compounds having larger unit cell parameters [98]. Also, it was found by Norby et al. that the difference in the electronegativities between B- and A-site cations, $\Delta\chi_{\text{B-A}}$, was found to be proportional to the enthalpy of hydration [98]. Thus, smaller $\Delta\chi_{\text{B-A}}$ should give rise to a higher equilibrium proton content. A review of the literature reveals several features that are characteristics of proton transport in perovskite-type oxides.

1. Proton conductivity is enhanced in wet atmospheres and occurs over a broad temperature range from room temperature to 700 °C encompassing the LT, IT, and HT regimes.

2. At the upper temperature region of the LT regime (zone 3), extending to the IT and HT regimes, the conductivity has additional contributions from oxygen ions due to the decreased water uptake with increasing temperature.
3. Grain boundary conductivity through various mechanisms outlined above dominates the behavior in LT (zones 1, 2, and 3), whereas bulk conductivity is predominant at higher temperatures.

Fluorite-type and simple oxides

Selected metal oxide hydrates like $\text{ZrO}_2 \cdot n\text{H}_2\text{O}$, $\text{Sb}_2\text{O}_5 \cdot n\text{H}_2\text{O}$ and $\text{WO}_3 \cdot 2\text{H}_2\text{O}$ have shown considerably high proton conductivity in the 50–150 °C region [106, 107]. The possibility of proton conduction in simple oxides (ZrO_2 , TiO_2 , CeO_2) at low temperature has been previously investigated. Conventional ceramic ionic conductors rely on bulk ionic transport, whereas a significant increase in the conductivity can be obtained when the grain size of the materials is in the nanometric range [108, 109]. Munir et al. [63] found the ionic conductivity at low temperatures (200 °C) in structurally un-hydrated YSZ only when the grain size of the material is in the nanoscale. Until recently, nanostructured YSZ was used as a low-temperature protonic conductor. The nanostructured YSZ made use of interfaces such as grain boundaries and surfaces resulting in appreciable proton conductivity at the interfacial hydrated layers [110], while bulk proton conduction in the solid lattice was negligible.

Figure 7 displays the proton conductivity of fluorite and simple oxides as a function of temperature in wet atmospheres. For fluorite-type YSZ, it was demonstrated that proton conductivity was significantly increased with a decrease in the grain size (from 100 nm to 10 nm) in the LT range (zone 1). Undoped ZrO_2 shows a similar behavior in the LT regime. Interestingly, Y_2O_3 concentration does not seem to have a significant impact on the protonic conductivity. However, doping of Y_2O_3 is known to have an effect on the concentration of oxygen vacancies, crystal structure, and particle morphology which helps determine water absorption and LT proton conduction. Shirpour et al. [25] compared the proton conductivity of microcrystalline (400 nm) and nanocrystalline (40 nm) ceria below 200 °C. Their result confirmed the existence of proton conductivity in nanocrystalline ceria at temperatures lower than 200 °C. Nanocrystalline samples exhibit more than eight orders of magnitude enhancement of total conductivity in wet atmosphere, which suggested unique properties of grain boundaries in such nanostructured materials.

Sun et al. [112] developed $\text{La}_2\text{Ce}_2\text{O}_7$ (LDC) with cubic fluorite crystal structure as a promising proton conductor. As shown in Fig. 7, the total conductivity of LDC is 4.5×10^{-5} at 250 °C in 3% H_2O -humidified air. Sun's work clearly showed that the environmental humidity could significantly affect the total conductivity of LDC, which could increase dramatically with increasing humidity. In addition, a proton transport number defined as the ratio of proton ionic conductivity to the total measured conductivity was measured to be approximately 0.89 at 250 °C in 3% H_2O -humidified air, indicating the proton transfer process played the dominant role under high water vapor pressure and low temperature [113]. Since protons are the main charge carriers at temperatures below 450 °C as demonstrated by Norby et al. [114, 115], LDC would be a promising proton conductor in the applications outlined in this review.

Brownmillerite type

Brownmillerite is a rare oxide mineral with chemical formula $\text{Ca}_2(\text{Al,Fe})_2\text{O}_5$. $\text{Ba}_2\text{In}_2\text{O}_5$ is a well-known oxide ion and proton-conductive material. Hui et al. reported the electrical conductivity of ceria-doped $\text{Ba}_2\text{In}_2\text{O}_5$ was significantly affected by the presence of hydrogen in the temperature range of 100–300 °C. As

shown in Fig. 8, the electrical conductivity was as high as 7×10^{-3} S/cm at 300 °C in an atmosphere of 50% hydrogen [116]. When BIS was applied as electrolyte materials with hydrogen as fuel, an open circuit voltage of 0.87 V was attained and was stable during an operation period of 60 h at 280 °C. The proton transfer numbers were measured to be around 0.86 at 100 °C, indicating BIC is a mixed electronic and ionic conductor. Due to the mixed electronic nature of conduction, these materials are promising candidates for use as electrodes in SOFCs.

Phosphate type

Low-temperature conduction in phosphate materials requires the presence of substantial amount of water enabling a vehicle transport mechanism. At high temperature, water should be removed from the structure and proton conduction can be attributed to a Grotthuss-type mechanism where proton hopping along P–O–H bonds occurs [117, 118]. Haile et al. demonstrated phosphate-type materials based on CsHSO_4 as fuel cell electrolytes with excellent performance [119–124]. Chen et al. [125] reported a proton and oxide co-ion conductor, $\text{Sn}_{0.9}\text{In}_{0.1}\text{P}_2\text{O}_7$. The maximum protonic conductivities of $\text{Sn}_{0.9}\text{In}_{0.1}\text{P}_2\text{O}_7$ achieved are 0.019 S/cm around 200 °C in 40% H_2O . The electrochemical properties of proton-conductive $\text{CsH}_2\text{PO}_4/\text{SiP}_2\text{O}_7$ composite were synthesized and investigated in the temperature range of 110–287 °C, and the maximum conductivity reached 44 mS/cm at 266 °C [124]. Figure 9 shows the conductivity of a SnP_2O_7 – SnO_2 composite. The conductivity increases with temperature and in wet atmosphere is higher than the level exhibited in dry atmospheres. An H/D isotope effect was observed for SnP_2O_7 which suggested that proton conduction in this material was based on a proton-hopping mechanism.

Other types

Although research into proton-conducting ceramics began more recently than oxide-ion conductors, several proton conductors described above have been identified that exhibit sufficient proton conductivity for use as electrolytes of PCFCs. In this section, we describe some new material systems that have been studied in the search for low-temperature proton conduction.

Figure 7 Proton conductivity of fluorite and simple oxides as a function of temperature in wet atmosphere. The solid line indicated extrapolation of the oxygen-ion conductivity of the 50 nm YSZ sample [34]. YSZ [24], CGO [35], undoped-ceria [25], TiO₂ [111], SDC and YSZ [61], La₂Ce₂O₇ [112].

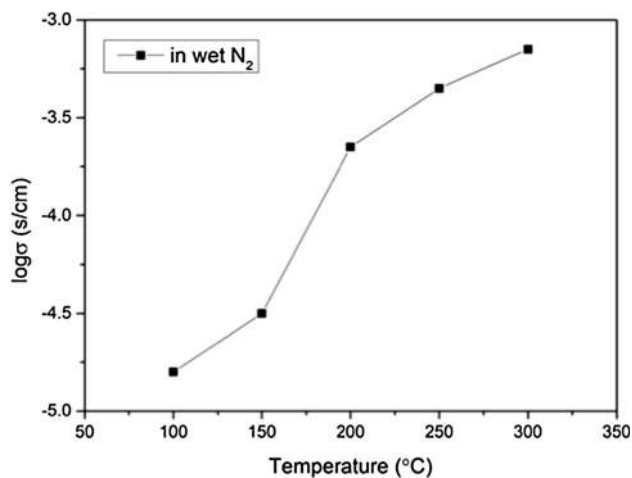
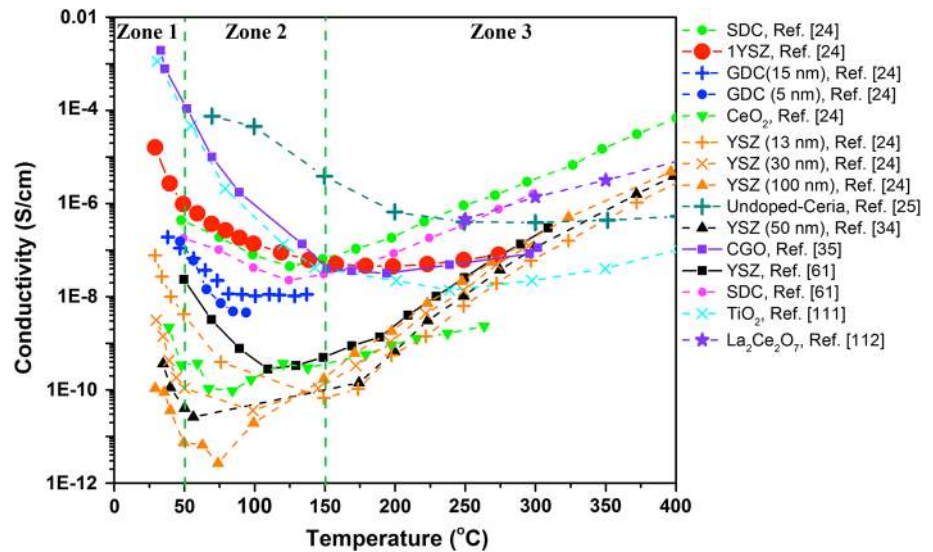


Figure 8 Proton conductivity of brownmillerite-type oxides ceria-doped Ba₂In₂O₅ as a function of temperature in wet atmosphere. Reprinted with permission from Hui et al. [116].

Aoki et al. [127] reported the proton conductivity of amorphous Al_nSi_{1-n}O_x thin film which has the heterogeneous nanoscale microstructure comprised of the ion-conducting, condensed glass microdomain and a poorly conductive, uncondensed glass microdomain. The proton conductivity reached 1.1×10^{-5} S/cm when the thickness was less than 5 nm at 250 °C. Dion–Jacobson (D-J)-type layered perovskite (ACa₂Nb₃O₁₀) oxides were developed by Sakthivel et al. as hydrogen gas sensors at a working temperature of 45 °C. The proton conductivity of KCa₂Nb₃O₁₀ (6.3×10^{-5} S/cm at 45 °C) was observed to be higher than analogs with Rb or Cs substituted on the A site. Kojo et al. [128] investigated

the influence of the La/W ratio on the electronic conductivity of lanthanum tungstate. When La/W = 6.5, the conductivity was 9.0×10^{-5} S/cm at 300 °C under wet Ar. Details of the temperature dependence over that LT regime defined in this review have not yet been reported.

Processing of nanocrystalline proton conductors

On the basis of the results described above, proton conduction occurs in polycrystalline samples with predominately nanometric-sized grains. One of the approaches to develop new low-temperature ionic

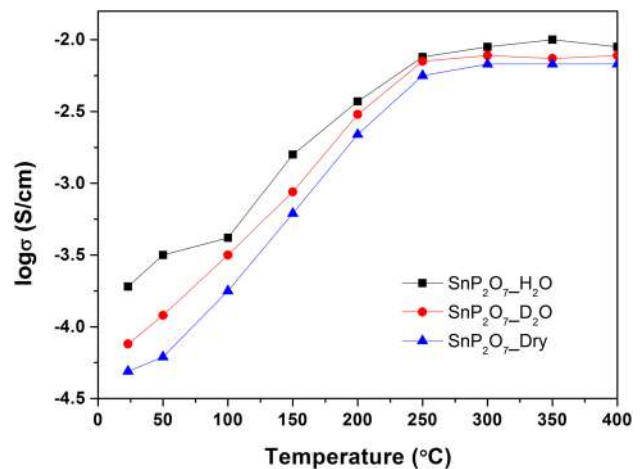


Figure 9 Temperature dependence of the conductivity of the SnP₂O₇-SnO₂ composite ceramic in various atmospheres [120], CeP₂O₇ [126].

conductors would be to increase the number of available interfaces such as grain boundaries and select surfaces that are favorable for hydration. Here, we will review several techniques which are available to process proton-conducting ceramics with the requisite grain sizes below 50 nm.

RT high-pressure compaction

Several nonconventional sintering approaches have been developed to fabricate nanostructured protonic ceramics. Miyoshi et al. fabricated nanograined YSZ through a combination of low-temperature nanopower synthesis and room-temperature high-pressure (4 GPa) compaction [24, 64]. The as-obtained samples after high-pressure compaction have grain size being typically smaller than 100 nm and have relatively good mechanical strength for handling and cutting. The relative density can reach 86% with limited nanopores. Those nanograined specimens essentially include interfacial hydrated layers between grains (Fig. 10), which were regarded to facilitate incorporation of H₂O molecules.

Hexamethylenetetramine (HMTA) or ultraviolet (UV) laser irradiation method

Takamura et al. successfully prepared single nano-sized 6 mol % Sm-doped ceria with a grain size of approximately 2 to 3 nm by using hexamethylenetetramine (HMTA) or ultraviolet (UV) laser irradiation method, with water adsorption of 3 mass% and 0.12 mass%, respectively [33]. As a result, the proton conductivity of as-obtained dense nanocrystalline ceria was about 10⁻⁷ to 10⁻⁸ S/cm at around 50 °C under humidified atmosphere (Fig. 11).

Hot pressing

A hot pressing method was applied by Weibel et al. [131] to prepare nanocrystalline TiO₂ ceramics. A density higher than 90% of the theoretical limit with a mean grain size of 30 nm was obtained at temperatures as low as 490 °C under 0.45 GPa for 2 h. Mazaheri et al. [130] adopted two-stage sintering to obtain titania nanograins assisted by the anatase-to-rutile phase transformation. At the end of the first sintering step, the minimum grain size was around 250 nm with a nearly complete anatase-to-rutile transformation (98% rutile). However, at the end of

the second step, the anatase-to-rutile transformation facilitated a reduction in grain size to ~ 100 nm. Even though the grain size was slightly larger than other sintering approaches, the two-step sintering features densification at a lower temperature without the application of external pressure.

Spark plasma sintering (SPS)

The SPS technique is similar to traditional hot pressing, but in SPS the sample is heated by a high-intensity and low-voltage pulsed DC current flowing through the sample and graphite die resulting in rapid heating [132]. The heating rate of SPS may be as fast as 100 °C/min, enabling rapid densification at very low temperatures with very short sintering times. Pérez-Coll et al. prepared dense nanocrystalline Ce_{0.9}Gd_{0.1}O_{2-δ} (CGO) with a grain size of ~ 120 nm by spark plasma sintering (SPS) of nanoscale powders [35]. Their result found that the large volume of grain boundaries in the nanometric materials are highly blocking oxygen ions but can promote proton transport through surface effects. The room-temperature proton conductivity of nanostructured Ce_{0.9}Gd_{0.1}O_{2-δ} is 4–5 times greater than that of micrometric samples. This group also prepared dense nanocrystalline YSZ with a grain size of ~ 50 nm and a density > 97% of the theoretical value by SPS [129]. Although samples prepared at relatively low pressures require high sintering temperature (800–1000 °C), SPS has been a proven method to successfully fabricate samples with nanoscale grain features. Hinterberg et al. [133] reported a spark-

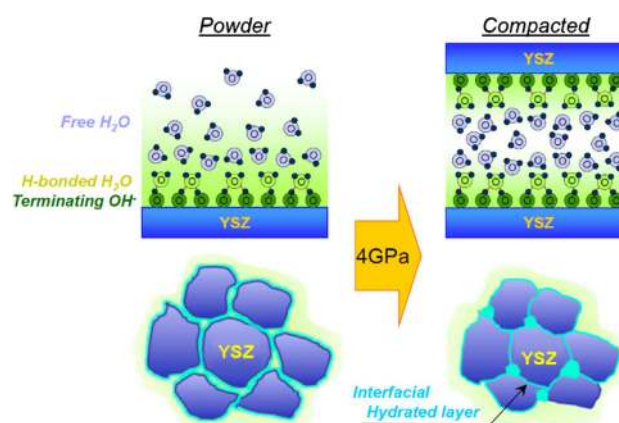
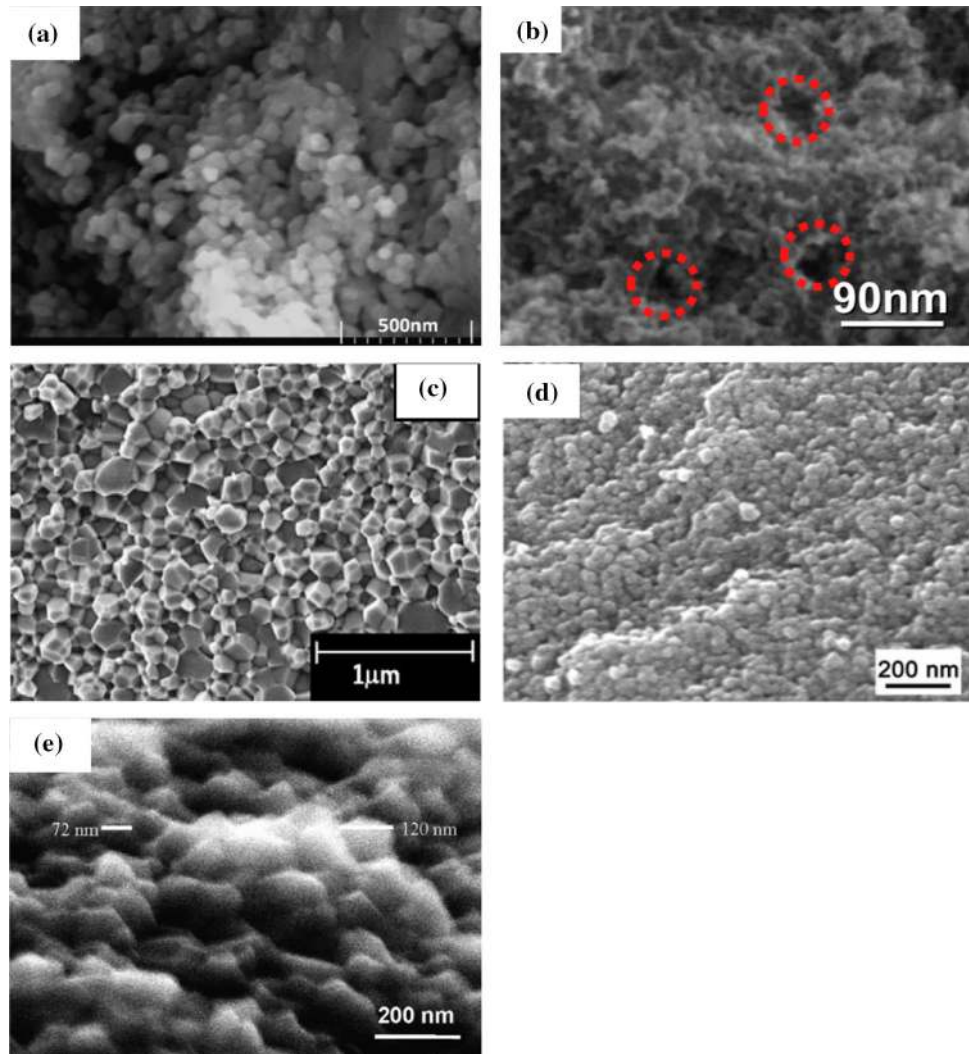


Figure 10 Schematic of the protonic species on nano grain surface (upper) and ultra-high-pressure compaction of nano grain (lower). Reprinted with permission from Miyoshi et al. [24].

Figure 11 SEM micrographs of the fractured surface of 8 mol% $\text{Y}_2\text{O}_3\text{-ZrO}_2$ (YSZ) by spark plasma sintering (a). 1YSZ specimen by room-temperature high-pressure (4 GPa) compaction (b). TiO_2 sample by two-step sintering process (c). On behalf of Acta Materialia Inc. anatase sample sintered at 550 °C by high-pressure field-assisted sintering (d). Phase-pure anatase by hot pressing (e) Reprinted with permission from Tandé et al. [129] (a), Miyoshi et al. [24] (b), Mazaheri et al. [130] (c), Maglia et al. [111] (d), Weibel et al. [131] (e).



plasma-sintered nanograined YSZ with a grain size (ca. 30 nm) and a relative density of 95.8% and higher. Spark-plasma-sintered YSZ with a grain size of 16 nm and relative density above 98% was reported by Chiodelli et al. [29] The high density of proton-conducting ceramics prepared by the SPS technique enables materials to be used as gas separation membranes and electrolyte materials at low temperature.

High-pressure field-assisted sintering method (HP-FAST)

Maglia et al. [111] prepared the high-density bulk anatase samples with a grain size ranging between 24 and 56 nm by high-pressure field-assisted sintering method (HP-FAST) which is operated at 550 °C under a pressure of 800 MPa. The sintered sample

appears to be free of residual inter-agglomerate porosity or cracks and has a good homogeneity of the grain-size distribution with limited presences of approximately 6 vol% nanopores.

LT-PCCs Applications

Proton exchange membranes

Recent research conducted by Sgabanikia et al. [136] showed that the introduction of nanosized $\text{La}_2\text{Ce}_2\text{O}_7$ into polybenzimidazole (PBI) membrane could increase the hydrophilicity of the polymer and modify the hydrophilic/hydrophobic properties of PLC_x (PBI/ $\text{La}_2\text{Ce}_2\text{O}_7$ nanocomposite membranes). $\text{La}_2\text{Ce}_2\text{O}_7$ can enhance the proton conductivity and the ion exchange capacity in the LT regime due to the

introduction of the LDC which provides additional hopping paths for proton transport.

Proton-conducting fuel cells

Kim et al. [31] showed the feasibility of power generation at room temperature using water concentration cells with nanoscale fluorite-structured oxides as electrolytes. They prepared dense, bulk nanostructured YSZ (8 mol% yttria) and SDC (20 mol% samaria) with a grain size of ~ 15 nm by field-activated sintering method. As shown in Fig. 12, a water concentration cell was constructed using the nanostructured YSZ and SDC as electrolytes. When one side of the cell was immersed into pure water and the other side was exposed to wet air, the *emf* reached about +110 mV and about +220 mV for the YSZ and SDC cells, respectively. In short circuit condition, a steady-state current of 6 nA was detected for SDC cell. Interestingly, the currents were three orders of magnitude lower for the microstructured YSZ and SDC electrolytes, indicating the essential role of interfacial proton transport.

Sensors

Sakthivel et al. [137] proposed a D–J-type proton conductor $\text{KCa}_2\text{Nb}_3\text{O}_{10}$ as hydrogen sensor. Deposition of Pt electrode on the top of the proton conductor was performed using the multistep impregnation–reduction method. A linear response current was observed at a hydrogen concentration of up to 5% and the same in the low ppm range (50–1000 ppm). A response time between 3 and 18 s was observed for H_2 concentration change in the range 1–7% at the temperature of 45 °C. This result indicates the possibility of development of a stable solid electrolyte-based sensor with excellent sensitivity and fast response time.

Perspective

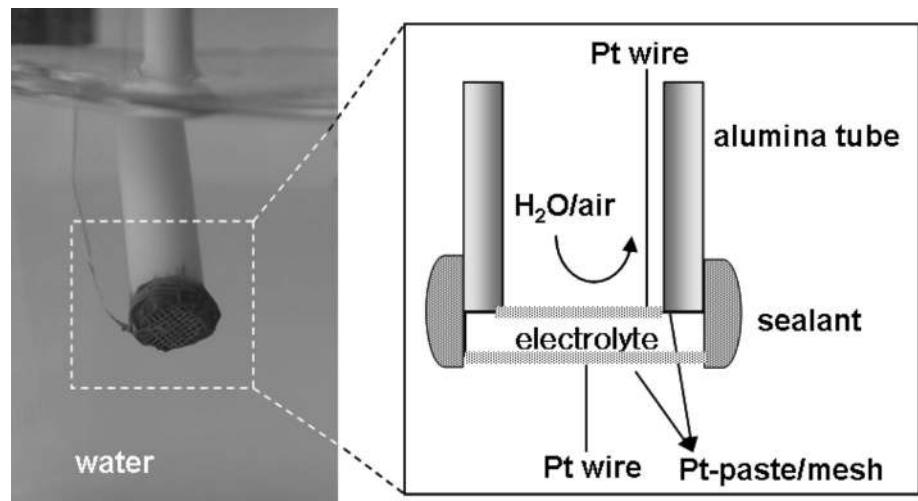
Low-temperature proton conduction (LT-PCCs), defined as operating in the temperature range of 25–400 °C was shown to depend on the material structure, temperature-dependent proton-conducting mechanisms, and microstructure indicating that interfacial protonic conduction dominates in the LT regime. Three temperature zones each possessed

interfacial conduction through different mechanisms. Zone 1, the lowest temperature region, was dominated by water absorption, dissociation, and a vehicle transport mechanism. Zone 2 extending from 50 to 150 °C was characterized by a transition from free water to bound water in the form of hydroxyl OH groups that experienced hopping mechanism at the interface. Zone 3 extending from 150 to above 400 °C was characterized by bulk incorporation and diffusion through hopping mechanism (Grotthuss) structures. From a materials perspective, essentially all the known materials exhibit the same qualitative trends in conductivity in zone 1 and zone 2 since water is known to absorb to a wide range of ceramic surfaces with an increased driving force with large surface areas inherent to nanostructured materials. However, zone 3 exhibits distinctly different behavior as a function of materials class since proton conduction is determined by incorporation and mobility of protonic species in the crystalline lattice. Perovskites incorporate protonic defects in wet atmospheres through oxygen vacancy sites, as compared to simple oxides such as TiO_2 which do not exhibit the capacity for bulk proton incorporation. Conductivities in zone 3 for simple oxides are related to electronic contributions to conductivity and contributions from oxygen ions as the temperature increases.

This review points to the importance of tailoring the surface chemical property and the potential doping strategies with alkaline earth metal ions to enhance the water absorption and proton mobility. Additional data are required for a wide range of materials in the LT regime, especially in zone 1 and zone 2 where water absorption and dissociation on surfaces are dominant. Computational studies focused on surface-dependent dissociative adsorption of water, and subsequent temperature-dependent transport would aid in materials discovery.

Finally, in addition to the role of hydrogen isotopes in evaluating the transport mechanism based on mass effects outlined earlier, hydrogen isotope transport in the LT regime may play an important role in capturing and processing of hydrogen isotopes. The low-temperature water adsorption properties of nanoscale structured ceramics outlined in this review could provide a low-cost and transformative avenue to address tritium management challenges. Enhanced understanding of LT proton transport materials and mechanisms would equivalently benefit energy conversion and storage applications based on solid oxide

Figure 12 Photograph and a schematic diagram of a water concentration cell operation at room temperature. Reprinted with permission from Kim et al. [31].



fuel cells, separation membranes, and associated sensors.

Acknowledgements

The authors gratefully acknowledge the Award DE-NE0008703 from the Department of Energy, Nuclear Energy Research Programs (DOE-NEUP) for Project CFA-17-12798: Nanostructured Ceramic Membranes for Enhanced Tritium Management.

Open Access This article is distributed under the terms of the Creative Commons Attribution 4.0 International License (<http://creativecommons.org/licenses/by/4.0/>), which permits unrestricted use, distribution, and reproduction in any medium, provided you give appropriate credit to the original author(s) and the source, provide a link to the Creative Commons license, and indicate if changes were made.

References

- [1] Fabbri E, Pergolesi D, Traversa E (2010) Materials challenges toward proton-conducting oxide fuel cells: a critical review. *Chem Soc Rev* 39:4355–4369. <https://doi.org/10.1039/b902343g>
- [2] Bi L, Da'as EH, Shafi SP (2017) Proton-conducting solid oxide fuel cell (SOFC) with Y-doped BaZrO₃ electrolyte. *Electrochem Commun* 80:20–23. <https://doi.org/10.1016/j.elecom.2017.05.006>
- [3] Shi Z, Sun W, Wang Z et al (2014) Samarium and Yttrium Codoped BaCeO₃ proton conductor with improved sinterability and higher electrical conductivity. *ACS Appl Mater Interfaces* 6:5175–5182. <https://doi.org/10.1021/am500467m>
- [4] Wang S, Shen J, Zhu Z et al (2018) Further optimization of barium cerate properties via co-doping strategy for potential application as proton-conducting solid oxide fuel cell electrolyte. *J Power Sour* 387:24–32. <https://doi.org/10.1016/j.jpowsour.2018.03.054>
- [5] Hou J, Miao L, Hui J et al (2018) A novel in situ diffusion strategy to fabricate high performance cathode for low temperature proton-conducting solid oxide fuel cells. *J Mater Chem A* 6:10411–10420. <https://doi.org/10.1039/C8TA00859K>
- [6] Clark D, Tong J, Morrissey A et al (2014) Anomalous low-temperature proton conductivity enhancement in a novel protonic nanocomposite. *Phys Chem Chem Phys* 16:5076–5080. <https://doi.org/10.1039/C4CP00468J>
- [7] Xu X, Bi L, Zhao XS (2018) Highly-conductive proton-conducting electrolyte membranes with a low sintering temperature for solid oxide fuel cells. *J Membr Sci* 558:17–25. <https://doi.org/10.1016/j.memsci.2018.04.037>
- [8] Wang B, Liu X, Bi L, Zhao XS (2019) Fabrication of high-performance proton-conducting electrolytes from microwave prepared ultrafine powders for solid oxide fuel cells. *J Power Sour* 412:664–669. <https://doi.org/10.1016/j.jpowsour.2018.11.051>
- [9] Xu N, Zhang C, Huang K (2018) Proton-mediated energy storage in intermediate-temperature solid-oxide metal–air batteries. *J Mater Chem A* 6:20659–20662. <https://doi.org/10.1039/C8TA08180H>
- [10] Hübert T, Boon-Brett L, Black G, Banach U (2011) Hydrogen sensors: a review. *Sens Actuators B Chem* 157:329–352. <https://doi.org/10.1016/j.snb.2011.04.070>

- [11] Tao Z, Yan L, Qiao J et al (2015) A review of advanced proton-conducting materials for hydrogen separation. *Prog Mater Sci* 74:1–50. <https://doi.org/10.1016/j.pmatsci.2015.04.002>
- [12] Kura C, Kunisada Y, Tsuji E et al (2017) Hydrogen separation by nanocrystalline titanium nitride membranes with high hydride ion conductivity. *Nat Energy* 2:786–794. <https://doi.org/10.1038/s41560-017-0002-2>
- [13] Wang H, Wang X, Meng B et al (2018) Perovskite-based mixed protonic–electronic conducting membranes for hydrogen separation: recent status and advances. *J Ind Eng Chem* 60:297–306. <https://doi.org/10.1016/j.jiec.2017.11.016>
- [14] Fang S, Wang S, Brinkman KS, Chen F (2014) A sinter-active Ni–BaZr_{0.8}Y_{0.2}O_{3–δ} composite membrane for hydrogen separation. *J Mater Chem A* 2:5825–5833. <https://doi.org/10.1039/c3ta14777k>
- [15] Liu M, Sun W, Li X et al (2013) High-performance Ni–BaZr_{0.1}Ce_{0.7}Y_{0.1}Yb_{0.1}O_{3–δ} (BZCYYb) membranes for hydrogen separation. *Int J Hydrogen Energy* 38:14743–14749. <https://doi.org/10.1016/j.ijhydene.2013.09.057>
- [16] Mukundan R (1999) Tritium conductivity and isotope effect in proton-conducting perovskites. *J Electrochem Soc* 146:2184–2187. <https://doi.org/10.1149/1.1391911>
- [17] Steele BCH, Heinzel A (2010) Materials for fuel-cell technologies. *Nature* 414:345–352
- [18] Wang S, Shen J, Zhu Z et al (2018) Further optimization of barium cerate properties via co-doping strategy for potential application as proton-conducting solid oxide fuel cell electrolyte. *J Power Sour* 387:24–32. <https://doi.org/10.1016/j.jpowsour.2018.03.054>
- [19] Zhu Z, Liu B, Shen J et al (2016) La₂Ce₂O₇: a promising proton ceramic conductor in hydrogen economy. *J Alloy Compd* 659:232–239. <https://doi.org/10.1016/j.jallcom.2015.11.041>
- [20] Zhang Y, Knibbe R, Sunarso J et al (2017) Recent progress on advanced materials for solid-oxide fuel cells operating below 500 °C. *Adv Mater* 29:1700132–1700164. <https://doi.org/10.1002/adma.201700132>
- [21] Marrony M (2016) Proton-conducting ceramics. CRC Press, Boca Raton
- [22] Kochetova N, Animitsa I, Medvedev D et al (2016) Recent activity in the development of proton-conducting oxides for high-temperature applications. *RSC Adv* 6:73222–73268. <https://doi.org/10.1039/C6RA13347A>
- [23] Wachsman ED, Lee KT (2011) Lowering the temperature of solid oxide fuel cells. *Science* 334:935–939. <https://doi.org/10.1126/science.1204090>
- [24] Miyoshi S, Akao Y, Kuwata N et al (2014) Low-temperature protonic conduction based on surface protonics: an example of nanostructured yttria-doped zirconia. *Chem Mater* 26:5194–5200. <https://doi.org/10.1021/cm5012923>
- [25] Shirpour M, Gregori G, Merkle R, Maier J (2011) On the proton conductivity in pure and gadolinium doped nanocrystalline cerium oxide. *Phys Chem Chem Phys* 13:937–940. <https://doi.org/10.1039/C0CP01702G>
- [26] Chiang Y-M, Lavik EB, Kosacki I et al (1996) Defect and transport properties of nanocrystalline CeO_{2–x}. *Appl Phys Lett* 69:185–187. <https://doi.org/10.1063/1.117366>
- [27] Park HJ, Roh JW (2016) Protonic conduction of nanostructured Y-Doped BaZrO₃. *J Nanomater* 2016:1–6. <https://doi.org/10.1155/2016/8757305>
- [28] Miyoshi S, Akao Y, Kuwata N et al (2014) Low-temperature protonic conduction based on surface protonics: an example of nanostructured yttria-doped zirconia. *Chem Mater* 26:5194–5200. <https://doi.org/10.1021/cm5012923>
- [29] Chiodelli G, Maglia F, Anselmi-Tamburini U, Munir ZA (2009) Characterization of low temperature protonic conductivity in bulk nanocrystalline fully stabilized zirconia. *Solid State Ion* 180:297–301. <https://doi.org/10.1016/j.ssi.2009.02.031>
- [30] Kim S, Avila-Paredes HJ, Wang S et al (2009) On the conduction pathway for protons in nanocrystalline yttria-stabilized zirconia. *Phys Chem Chem Phys* 11:3035–3038. <https://doi.org/10.1039/b901623f>
- [31] Kim S, Anselmi-Tamburini U, Park HJ et al (2008) Unprecedented room-temperature electrical power generation using nanoscale fluorite-structured oxide electrolytes. *Adv Mater* 20:556–559. <https://doi.org/10.1002/adma.200700715>
- [32] Gregori G, Shirpour M, Maier J (2013) Proton conduction in dense and porous nanocrystalline ceria thin films. *Adv Funct Mater* 23:5861–5867. <https://doi.org/10.1002/adfm.201300527>
- [33] Takamura H, Takahashi N (2010) Electrical conductivity of dense nanocrystalline ceria under humidified atmosphere. *Solid State Ion* 181:100–103. <https://doi.org/10.1016/j.ssi.2009.04.017>
- [34] Avila-Paredes HJ, Zhao J, Wang S et al (2010) Protonic conductivity of nano-structured Yttria-stabilized zirconia: dependence on grain size. *J Mater Chem* 20:990–994. <https://doi.org/10.1039/B919100C>
- [35] Pérez-Coll D, Mather GC (2010) Electrical transport at low temperatures in dense nanocrystalline Gd-doped ceria. *Solid State Ion* 181:1033–1042. <https://doi.org/10.1016/j.ssi.2009.11.017>

- [36] Ruiz-Trejo E, Kilner JA (2009) Possible proton conduction in $\text{Ce}_{0.9}\text{Gd}_{0.1}\text{O}_{2-\delta}$ nanoceramics. *J Appl Electrochem* 39:523–528. <https://doi.org/10.1007/s10800-008-9713-1>
- [37] Maglia F, Tredici IG, Spinolo G, Anselmi-Tamburini U (2012) Low temperature proton conduction in bulk nanometric TiO_2 prepared by high-pressure field assisted sintering. *J Mater Res* 27:1975–1981. <https://doi.org/10.1557/jmr.2012.158>
- [38] Gui D, Zheng T, Xie J et al (2016) Significantly dense two-dimensional hydrogen-bond network in a layered zirconium phosphate leading to high proton conductivities in both water-assisted low-temperature and anhydrous intermediate-temperature regions. *Inorg Chem* 55:12508–12511. <https://doi.org/10.1021/acs.inorgchem.6b02308>
- [39] Dobrovolsky Y, Leonova L, Nadkhina S, Panina N (1999) Low-temperature proton conductivity in hydrated and nonhydrated tin dioxide. *Solid State Ion* 119:275–279. [https://doi.org/10.1016/S0167-2738\(98\)00514-1](https://doi.org/10.1016/S0167-2738(98)00514-1)
- [40] Wei T, Zhang LA, Chen Y et al (2017) Promising proton conductor for intermediate-temperature fuel cells: $\text{Li}_{13.9}\text{Sr}_{0.1}\text{Zn}(\text{GeO}_4)_4$. *Chem Mater* 29:1490–1495. <https://doi.org/10.1021/acs.chemmater.6b03471>
- [41] Zhou Y, Guan X, Zhou H et al (2016) Strongly correlated perovskite fuel cells. *Nature* 534:231–234. <https://doi.org/10.1038/nature17653>
- [42] Brunauer S, Emmett PH, Teller E (1938) Adsorption of gases in multimolecular layers. *J Am Chem Soc* 60:309–319. <https://doi.org/10.1021/ja01269a023>
- [43] Langmuir I (1916) the constitution and fundamental properties of solids and liquids. Part I solids. *J Am Chem Soc* 38:2221–2295. <https://doi.org/10.1021/ja02268a002>
- [44] Stub SØ, Vøllestad E, Norby T (2017) Mechanisms of protonic surface transport in porous oxides: example of YSZ. *J Phys Chem C* 121:12817–12825. <https://doi.org/10.1021/acs.jpcc.7b03005>
- [45] Asay DB, Kim SH (2005) Evolution of the adsorbed water layer structure on silicon oxide at room temperature. *J Phys Chem B* 109:16760–16763. <https://doi.org/10.1021/jp053042o>
- [46] Kreuer K (1999) Aspects of the formation and mobility of protonic charge carriers and the stability of perovskite-type oxides. *Solid State Ion* 125:285–302. [https://doi.org/10.1016/S0167-2738\(99\)00188-5](https://doi.org/10.1016/S0167-2738(99)00188-5)
- [47] Kreuer K (1995) H/D isotope effect of proton conductivity and proton conduction mechanism in oxides. *Solid State Ion* 77:157–162. [https://doi.org/10.1016/0167-2738\(94\)00265-T](https://doi.org/10.1016/0167-2738(94)00265-T)
- [48] Świerczek K, Skubida W (2017) Optimization of proton conductors for application in solid oxide fuel cell technology. *E3S Web Conf* 14:01044–01054. <https://doi.org/10.1051/e3sconf/20171401044>
- [49] Nowick A, Vaysleyb A (1997) Isotope effect and proton hopping in high-temperature protonic conductors. *Solid State Ion* 97:17–26. [https://doi.org/10.1016/S0167-2738\(97\)00081-7](https://doi.org/10.1016/S0167-2738(97)00081-7)
- [50] Bonanos N, Huijser A, Poulsen FW (2015) H/D isotope effects in high temperature proton conductors. *Solid State Ion* 275:9–13. <https://doi.org/10.1016/j.ssi.2015.03.028>
- [51] Uchida H (1989) Formation of protons in SrCeO_3 -based proton conducting oxides. Part II. Evaluation of proton concentration and mobility in Yb-doped SrCeO_3 . *Solid State Ion* 36:89–95. [https://doi.org/10.1016/0167-2738\(89\)90065-9](https://doi.org/10.1016/0167-2738(89)90065-9)
- [52] Bonanos N (2001) Oxide-based protonic conductors: point defects and transport properties. *Solid State Ion* 145:265–274. [https://doi.org/10.1016/S0167-2738\(01\)00951-1](https://doi.org/10.1016/S0167-2738(01)00951-1)
- [53] Nowick A (1995) High-temperature protonic conductors with perovskite-related structures. *Solid State Ion* 77:137–146. [https://doi.org/10.1016/0167-2738\(94\)00230-P](https://doi.org/10.1016/0167-2738(94)00230-P)
- [54] Kreuer KD, Adams S, Münch W et al (2001) Proton conducting alkaline earth zirconates and titanates for high drain electrochemical applications. *Solid State Ion* 145:295–306. [https://doi.org/10.1016/S0167-2738\(01\)00953-5](https://doi.org/10.1016/S0167-2738(01)00953-5)
- [55] Yamazaki Y, Babilo P, Haile SM (2008) Defect chemistry of Yttrium-doped barium zirconate: a thermodynamic analysis of water uptake. *Chem Mater* 20:6352–6357. <https://doi.org/10.1021/cm800843s>
- [56] Haile SM, Staneff G, Ryu KH (2001) Non-stoichiometry, grain boundary transport and chemical stability of proton conducting perovskites. *J Mater Sci* 36:1149–1160. <https://doi.org/10.1023/A:1004877708871>
- [57] Kreuer KD (2003) Proton-conducting oxides. *Ann Rev Mater Res* 33:333–359. <https://doi.org/10.1146/annurev.matsci.33.022802.091825>
- [58] Uchida H (1983) Relation between proton and hole conduction in SrCeO_3 -based solid electrolytes under water-containing atmospheres at high temperatures. *Solid State Ion* 11:117–124. [https://doi.org/10.1016/0167-2738\(83\)90048-6](https://doi.org/10.1016/0167-2738(83)90048-6)
- [59] Malavasi L, Fisher CAJ, Islam MS (2010) Oxide-ion and proton conducting electrolyte materials for clean energy applications: structural and mechanistic features. *Chem Soc Rev* 39:4370–4387. <https://doi.org/10.1039/b915141a>
- [60] Bielecki J, Parker SF, Mazzei L et al (2016) Structure and dehydration mechanism of the proton conducting oxide $\text{Ba}_2\text{In}_2\text{O}_5(\text{H}_2\text{O})_x$. *J Mater Chem A* 4:1224–1232. <https://doi.org/10.1039/C5TA05728K>

- [61] Avila-Paredes HJ, Barrera-Calva E, Anderson HU et al (2010) Room-temperature protonic conduction in nanocrystalline films of yttria-stabilized zirconia. *J Mater Chem* 20:6235–6238. <https://doi.org/10.1039/c0jm00051e>
- [62] Guo X (1999) On the degradation of zirconia ceramics during low-temperature annealing in water or water vapor. *J Phys Chem Solids* 60:539–546. [https://doi.org/10.1016/S0022-3697\(98\)00301-1](https://doi.org/10.1016/S0022-3697(98)00301-1)
- [63] Anselmi-Tamburini U, Maglia F, Chiodelli G et al (2006) Enhanced low-temperature protonic conductivity in fully dense nanometric cubic Zirconia. *Appl Phys Lett* 89:163116–163118. <https://doi.org/10.1063/1.2360934>
- [64] Miyoshi S, Akao Y, Kuwata N et al (2012) Water uptake and conduction property of nano-grained yttria-doped zirconia fabricated by ultra-high pressure compaction at room temperature. *Solid State Ion* 207:21–28. <https://doi.org/10.1016/j.ssi.2011.11.014>
- [65] Jing Y, Matsumoto H, Aluru NR (2018) Mechanistic insights into hydration of solid oxides. *Chem Mater* 30:138–144. <https://doi.org/10.1021/acs.chemmater.7b03476>
- [66] Tret'yakov NE, Filimonov VN (1972) Relative proton-donor capacity of hydroxyl groups of surface oxides studied by an ir-spectroscopic method. *Kinet Katal* 13:815–823
- [67] Holmes HF, Fuller EL, Gammage RB (1972) Heats of immersion in the zirconium oxide-water system. *J Phys Chem* 76:1497–1502. <https://doi.org/10.1021/j100654a023>
- [68] Yamada M, Wei M, Honma I, Zhou H (2006) One-dimensional proton conductor under high vapor pressure condition employing titanate nanotube. *Electrochem Commun* 8:1549–1552. <https://doi.org/10.1016/j.elecom.2006.07.020>
- [69] Iwahara H, Esaka T, Uchida H, Maeda N (1981) Proton conduction in sintered oxides and its application to steam electrolysis for hydrogen production. *Solid State Ion* 3–4:359–363. [https://doi.org/10.1016/0167-2738\(81\)90113-2](https://doi.org/10.1016/0167-2738(81)90113-2)
- [70] Norby T (1999) Solid-state protonic conductors: principles, properties, progress and prospects. *Solid State Ion* 125:1–11. [https://doi.org/10.1016/S0167-2738\(99\)00152-6](https://doi.org/10.1016/S0167-2738(99)00152-6)
- [71] Iwahara H (1996) Proton conducting ceramics and their applications. *Solid State Ion* 86–88:9–15. [https://doi.org/10.1016/0167-2738\(96\)00087-2](https://doi.org/10.1016/0167-2738(96)00087-2)
- [72] Haile SM, West DL, Campbell J (1998) The role of microstructure and processing on the proton conducting properties of gadolinium-doped barium cerate. *J Mater Res* 13:1576–1595. <https://doi.org/10.1557/JMR.1998.0219>
- [73] Christie G (1996) Microstructure: ionic conductivity relationships in ceria-gadolinia electrolytes. *Solid State Ion* 83:17–27. [https://doi.org/10.1016/0167-2738\(95\)00155-7](https://doi.org/10.1016/0167-2738(95)00155-7)
- [74] Nafe H (1984) Ionic conductivity of ThO₂- and ZrO₂-based electrolytes between 300 and 2000 K. *Solid State Ion* 13:255–263. [https://doi.org/10.1016/0167-2738\(84\)90040-7](https://doi.org/10.1016/0167-2738(84)90040-7)
- [75] Braun A, Duval S, Ried P et al (2009) Proton diffusivity in the BaZr_{0.9}Y_{0.1}O_{3-δ} proton conductor. *J Appl Electrochem* 39:471–475. <https://doi.org/10.1007/s10800-008-9667-3>
- [76] Shirpour M, Merkle R, Lin CT, Maier J (2012) Nonlinear electrical grain boundary properties in proton conducting Y-BaZrO₃ supporting the space charge depletion model. *Phys Chem Chem Phys* 14:730–740. <https://doi.org/10.1039/C1CP22487E>
- [77] Kjøseth C, Fjeld H, Prytz Ø et al (2010) Space-charge theory applied to the grain boundary impedance of proton conducting BaZr_{0.9}Y_{0.1}O_{3-δ}. *Solid State Ion* 181:268–275. <https://doi.org/10.1016/j.ssi.2010.01.014>
- [78] Park HJ, Kwak C, Lee KH et al (2009) Interfacial protonic conduction in ceramics. *J Eur Ceram Soc* 29:2429–2437. <https://doi.org/10.1016/j.jeurceramsoc.2009.02.010>
- [79] Guo X, Waser R (2006) Electrical properties of the grain boundaries of oxygen ion conductors: acceptor-doped zirconia and ceria. *Prog Mater Sci* 51:151–210. <https://doi.org/10.1016/j.pmatsci.2005.07.001>
- [80] Kliewer KL, Koehler JS (1965) Space charge in ionic crystals. I. General approach with application to NaCl. *Phys Rev* 140:A1226–A1240. <https://doi.org/10.1103/PhysRev.140.A1226>
- [81] Guo X, Maier J (2001) Grain boundary blocking effect in Zirconia: a Schottky barrier analysis. *J Electrochem Soc* 148:E121–E126. <https://doi.org/10.1149/1.1348267>
- [82] Lee JS, Anselmi-Tamburini U, Munir ZA, Kim S (2006) Direct evidence of electron accumulation in the grain boundary of yttria-doped nanocrystalline Zirconia ceramics. *Electrochem Solid-State Lett* 9:J34–J36. <https://doi.org/10.1149/1.2208012>
- [83] De Souza RA, Pietrowski MJ, Anselmi-Tamburini U et al (2008) Oxygen diffusion in nanocrystalline yttria-stabilized zirconia: the effect of grain boundaries. *Phys Chem Chem Phys* 10:2067. <https://doi.org/10.1039/b719363g>
- [84] Tschöpe A (2001) Grain size-dependent electrical conductivity of polycrystalline cerium oxide II: space charge model. *Solid State Ion* 139:267–280. [https://doi.org/10.1016/S0167-2738\(01\)00677-4](https://doi.org/10.1016/S0167-2738(01)00677-4)
- [85] Kim S, Fleig J, Maier J (2003) Space charge conduction: simple analytical solutions for ionic and mixed conductors and application to nanocrystalline ceria. *Phys Chem Chem Phys* 5:2268–2273. <https://doi.org/10.1039/B300170A>
- [86] Iwahara H, Yajima T, Hibino T et al (1993) Protonic conduction in calcium, strontium and barium zirconates. *Solid*

- State Ion 61:65–69. [https://doi.org/10.1016/0167-2738\(93\)90335-Z](https://doi.org/10.1016/0167-2738(93)90335-Z)
- [87] Yajima T, Suzuki H, Yogo T, Iwahara H (1992) Protonic conduction in SrZrO₃-based oxides. *Solid State Ion* 51:101–107. [https://doi.org/10.1016/0167-2738\(92\)90351-O](https://doi.org/10.1016/0167-2738(92)90351-O)
- [88] Yajima T, Kazeoka H, Yogo T, Iwahara H (1991) Proton conduction in sintered oxides based on CaZrO₃. *Solid State Ion* 47:271–275. [https://doi.org/10.1016/0167-2738\(91\)90249-B](https://doi.org/10.1016/0167-2738(91)90249-B)
- [89] Münch W, Kreuer KD, Adams et al (1999) The relation between crystal structure and the formation and mobility of protonic charge carriers in perovskite-type oxides: a case study of Y-doped BaCeO₃ and SrCeO₃. *Phase Trans* 68:567–586. <https://doi.org/10.1080/01411599908224535>
- [90] Singh K, Kannan R, Thangadurai V (2016) Synthesis and characterisation of ceramic proton conducting perovskite-type multi-element-doped Ba_{0.5}Sr_{0.5}Ce_{1-x-y-z}Zr_xGd_yY_zO_{3-δ} (0 < x < 0.5; y = 0, 0.1, 0.15; z = 0.1, 0.2). *Int J Hydrogen Energy* 41:13227–13237. <https://doi.org/10.1016/j.ijhydene.2016.05.089>
- [91] Corcoran DJ, Irvine JT (2001) Investigations into Sr₃CaZr_{0.5}Ta_{1.5}O_{8.75}, a novel proton conducting perovskite oxide. *Solid State Ion* 145:307–313. [https://doi.org/10.1016/S0167-2738\(01\)00955-9](https://doi.org/10.1016/S0167-2738(01)00955-9)
- [92] Ahmed I, Eriksson S, Ahlberg E et al (2006) Synthesis and structural characterization of perovskite type proton conducting BaZr_{1-x}In_xO_{3-δ} (0.0 ≤ x ≤ 0.75). *Solid State Ion* 177:1395–1403. <https://doi.org/10.1016/j.ssi.2006.07.009>
- [93] Ding H, Lin B, Fang D et al (2009) BaZr_{0.1}Ce_{0.7}Y_{0.2}O_{3-δ} proton-conducting electrolyte prepared by gel-casting for low-temperature solid oxide fuel cells. *J Alloy Compd* 474:364–369. <https://doi.org/10.1016/j.jallcom.2008.06.106>
- [94] Khani Z, Taillades-Jacquín M, Taillades G et al (2009) New synthesis of nanopowders of proton conducting materials. A route to densified proton ceramics. *J Solid State Chem* 182:790–798. <https://doi.org/10.1016/j.jssc.2008.12.020>
- [95] Ahmed I, Kinyanjui FG, Steegstra P et al (2010) Improved proton conductivity in spark-plasma sintered dense ceramic BaZr_{0.5}In_{0.5}O_{3-δ}. *Electrochem Solid State Lett* 13:B130–B134. <https://doi.org/10.1149/1.3482016>
- [96] Barison S, Battagliarin M, Cavallin T et al (2008) Barium non-stoichiometry role on the properties of Ba_{1+x}Ce_{0.65}Zr_{0.20}Y_{0.15}O_{3-δ} proton conductors for IT-SOFCs. *Fuel Cells* 8:360–368. <https://doi.org/10.1002/fuce.200800021>
- [97] Świerczek K, Skubida W, Niemczyk A et al (2017) Structure and transport properties of proton-conducting BaSn_{0.5}In_{0.5}O_{2.75} and A-site substituted Ba_{0.9}Ln_{0.1}Sn_{0.5}In_{0.5}O_{2.8} (Ln = La, Gd) oxides. *Solid State Ion* 307:44–50. <https://doi.org/10.1016/j.ssi.2017.05.010>
- [98] Świerczek K, Zajac W, Klimkowicz A et al (2015) Crystal structure and proton conductivity in highly oxygen-deficient Ba_{1-x}La_x(In, Zr, Sn)O_{3-δ} perovskites. *Solid State Ion* 275:58–61. <https://doi.org/10.1016/j.ssi.2015.02.018>
- [99] Bohn HG, Schober T (2000) Electrical conductivity of the high-temperature proton conductor BaZr_{0.9}Y_{0.1}O_{2.95}. *J Am Ceram Soc* 83:768–772. <https://doi.org/10.1111/j.1151-2916.2000.tb01272.x>
- [100] Iguchi F, Sata N, Tsurui T, Yugami H (2007) Microstructures and grain boundary conductivity of BaZr_{1-x}Y_xO₃ (x = 0.05, 0.10, 0.15) ceramics. *Solid State Ion* 178:691–695. <https://doi.org/10.1016/j.ssi.2007.02.019>
- [101] Cervera R, Oyama Y, Miyoshi S et al (2008) Structural study and proton transport of bulk nanograined Y-doped BaZrO₃ oxide protonics materials. *Solid State Ion* 179:236–242. <https://doi.org/10.1016/j.ssi.2008.01.082>
- [102] Tao S, Irvine JTS (2007) Conductivity studies of dense yttrium-doped BaZrO₃ sintered at 1325 °C. *J Solid State Chem* 180:3493–3503. <https://doi.org/10.1016/j.jssc.2007.09.027>
- [103] Ryu KH, Haile SM (1999) Chemical stability and proton conductivity of doped BaCeO₃–BaZrO₃ solid solutions. *Solid State Ion* 125:355–367. [https://doi.org/10.1016/S0167-2738\(99\)00196-4](https://doi.org/10.1016/S0167-2738(99)00196-4)
- [104] Azad A, Irvine J (2007) Synthesis, chemical stability and proton conductivity of the perovskites Ba(Ce, Zr)_{1-x}Sc_xO_{3-δ}. *Solid State Ion* 178:635–640. <https://doi.org/10.1016/j.ssi.2007.02.004>
- [105] Potter A, Baker R (2006) Impedance studies on Pt |SrCe_{0.95}Yb_{0.05}O₃| Pt under dried and humidified air, argon and hydrogen. *Solid State Ion* 177:1917–1924. <https://doi.org/10.1016/j.ssi.2006.06.022>
- [106] Li YM, Hibino M, Miyayama M, Kudo T (2000) Proton conductivity of tungsten trioxide hydrates at intermediate temperature. *Solid State Ion* 134:271–279
- [107] England W, Cross M, Hamnett A et al (1980) Fast proton conduction in inorganic ion-exchange compounds. *Solid State Ion* 1:231–249. [https://doi.org/10.1016/0167-2738\(80\)90007-7](https://doi.org/10.1016/0167-2738(80)90007-7)
- [108] Schoonman J (2000) Nanostructured materials in solid state ionics. *Solid State Ion* 135:5–19. [https://doi.org/10.1016/S0167-2738\(00\)00324-6](https://doi.org/10.1016/S0167-2738(00)00324-6)
- [109] Tuller H (2000) Ionic conduction in nanocrystalline materials. *Solid State Ion* 131:143–157. [https://doi.org/10.1016/S0167-2738\(00\)00629-9](https://doi.org/10.1016/S0167-2738(00)00629-9)
- [110] Dawson JA, Tanaka I (2014) Proton incorporation and trapping in ZrO₂ grain boundaries. *J Mater Chem A* 2:1400–1408. <https://doi.org/10.1039/C3TA14029F>

- [111] Maglia F, Tredici IG, Spinolo G, Anselmi-Tamburini U (2012) Low temperature proton conduction in bulk nanometric TiO₂ prepared by high-pressure field assisted sintering. *J Mater Res* 27:1975–1981. <https://doi.org/10.1557/jmr.2012.158>
- [112] Sun W, Fang S, Yan L, Liu W (2012) Investigation on proton conductivity of La₂Ce₂O₇ in wet atmosphere: dependence on water vapor partial pressure. *Fuel Cells* 12:457–463. <https://doi.org/10.1002/fuce.201100175>
- [113] Zhu Z, Liu B, Shen J et al (2016) La₂Ce₂O₇: a promising proton ceramic conductor in hydrogen economy. *J Alloy Compd* 659:232–239. <https://doi.org/10.1016/j.jallcom.2015.11.041>
- [114] Besikiotis V, Knee CS, Ahmed I et al (2012) Crystal structure, hydration and ionic conductivity of the inherently oxygen-deficient La₂Ce₂O₇. *Solid State Ion* 228:1–7. <https://doi.org/10.1016/j.ssi.2012.08.023>
- [115] Besikiotis V, Ricote S, Jensen MH et al (2012) Conductivity and hydration trends in disordered fluorite and pyrochlore oxides: a study on lanthanum cerate–zirconate based compounds. *Solid State Ion* 229:26–32. <https://doi.org/10.1016/j.ssi.2012.10.004>
- [116] Hui R, Maric R, Decès-Petit C et al (2006) Proton conduction in ceria-doped Ba₂In₂O₅ nanocrystalline ceramic at low temperature. *J Power Sour* 161:40–46. <https://doi.org/10.1016/j.jpowsour.2006.03.070>
- [117] Nogami M, Matsushita H, Goto Y, Kasuga T (2000) A sol-gel-derived glass as a fuel cell electrolyte. *Adv Mater* 12:1370–1372. [https://doi.org/10.1002/1521-4095\(200009\)12:18%3c1370:AID-ADMA1370%3e3.0.CO;2-1](https://doi.org/10.1002/1521-4095(200009)12:18%3c1370:AID-ADMA1370%3e3.0.CO;2-1)
- [118] Uma T, Nogami M (2006) On the development of proton conducting P₂O₅–ZrO₂–SiO₂ glasses for fuel cell electrolytes. *Mater Chem Phys* 98:382–388. <https://doi.org/10.1016/j.matchemphys.2005.09.049>
- [119] Haile SM, Boysen DA, Chisholm CRI, Merle RB (2001) Solid acids as fuel cell electrolytes. *Nature* 410:910–913. <https://doi.org/10.1038/35073536>
- [120] Shen Y, Nishida M, Kanematsu W, Hibino T (2011) Synthesis and characterization of dense SnP₂O₇–SnO₂ composite ceramics as intermediate-temperature proton conductors. *J Mater Chem* 21:663–670. <https://doi.org/10.1039/C0JM02596H>
- [121] Xu X, Tao S, Wormald P, Irvine JTS (2010) Intermediate temperature stable proton conductors based upon SnP₂O₇, including additional H₃PO₄. *J Mater Chem* 20:7827. <https://doi.org/10.1039/c0jm01089h>
- [122] Paschos O, Kunze J, Stimming U, Maglia F (2011) A review on phosphate based, solid state, protonic conductors for intermediate temperature fuel cells. *J Phys Condens Matter* 23:234110–234135. <https://doi.org/10.1088/0953-984/23/23/234110>
- [123] Martsinkevich VV, Ponomareva VG (2012) Double salts Cs_{1-x}M_xH₂PO₄ (M = Na, K, Rb) as proton conductors. *Solid State Ion* 225:236–240. <https://doi.org/10.1016/j.ssi.2012.04.016>
- [124] Matsui T, Kukino T, Kikuchi R, Eguchi K (2005) An intermediate temperature proton-conducting electrolyte based on a CsH₂PO₄/SiP₂O₇ composite. *Electrochem Solid-State Lett* 8:A256–A258. <https://doi.org/10.1149/1.1883906>
- [125] Chen X, Wang C, Payzant EA et al (2008) An oxide ion and proton Co-ion conducting Sn_{0.9}In_{0.1}P₂O₇ electrolyte for intermediate-temperature fuel cells. *J Electrochem Soc* 155:B1264–B1269. <https://doi.org/10.1149/1.2988135>
- [126] Le M-V, Tsai D-S, Yang C-Y et al (2011) Proton conductors of cerium pyrophosphate for intermediate temperature fuel cell. *Electrochim Acta* 56:6654–6660. <https://doi.org/10.1016/j.electacta.2011.05.040>
- [127] Aoki Y, Harada A, Nakao A et al (2012) Percolative proton conductivity of sol–gel derived amorphous aluminosilicate thin films. *Phys Chem Chem Phys* 14:2735–2742. <https://doi.org/10.1039/c2cp23821g>
- [128] Kojima G, Shono Y, Ushiyama H et al (2017) Influence of La/W ratio on electrical conductivity of lanthanum tungstate with high La/W ratio. *J Solid State Chem* 248:1–8. <https://doi.org/10.1016/j.jssc.2017.01.011>
- [129] Tandé C, Pérez-Coll D, Mather GC (2012) Surface proton conductivity of dense nanocrystalline YSZ. *J Mater Chem* 22:11208. <https://doi.org/10.1039/c2jm31414b>
- [130] Mazaheri M, Razavi Hesabi Z, Sadmezhad SK (2008) Two-step sintering of titania nanoceramics assisted by anatase-to-rutile phase transformation. *Scripta Mater* 59:139–142. <https://doi.org/10.1016/j.scriptamat.2008.02.041>
- [131] Weibel A, Bouchet R, Denoyel R, Knauth P (2007) Hot pressing of nanocrystalline TiO₂ (anatase) ceramics with controlled microstructure. *J Eur Ceram Soc* 27:2641–2646. <https://doi.org/10.1016/j.jeurceramsoc.2006.11.073>
- [132] Anselmi-Tamburini U, Garay JE, Munir ZA (2006) Fast low-temperature consolidation of bulk nanometric ceramic materials. *Scripta Mater* 54:823–828. <https://doi.org/10.1016/j.scriptamat.2005.11.015>
- [133] Hinterberg J, Adams A, Blümich B et al (2013) 1H-NMR measurements of proton mobility in nano-crystalline YSZ. *Phys Chem Chem Phys* 15:19825–19830. <https://doi.org/10.1039/c3cp53039f>
- [134] Buscaglia V, Viviani M, Buscaglia MT et al (2004) Nanostructured barium titanate ceramics. *Powder Technol* 148:24–27. <https://doi.org/10.1016/j.powtec.2004.09.016>

- [135] Xiao CJ, Li ZX, Deng XR (2011) Grain-size effects on thermal properties of BaTiO₃ ceramics. *Bull Mater Sci* 34:963–966. <https://doi.org/10.1007/s12034-011-0222-1>
- [136] Shabanikia A, Javanbakht M, Amoli HS et al (2014) Effect of La₂Ce₂O₇ on the physicochemical properties of phosphoric acid doped polybenzimidazole nanocomposite membranes for high temperature proton exchange membrane fuel cells applications. *J Electrochem Soc* 161:F1403–F1408. <https://doi.org/10.1149/2.0561414jes>
- [137] Sakthivel M, Weppner W (2007) Hydrogen sensing based on proton and electron transport across and along the interface solid oxide electrolyte–platinum electrode. *J Phys D Appl Phys* 40:7210–7216. <https://doi.org/10.1088/0022-3727/40/23/S04>
- [138] Kreuer KD (2003) Proton-conducting oxides. *Ann Rev Mater Res* 33:333–359. <https://doi.org/10.1146/annurev.matsci.33.022802.091825>

Publisher's Note Springer Nature remains neutral with regard to jurisdictional claims in published maps and institutional affiliations.